
Characterisation of Model Peptides QKFFFDQ and QDFFFKQ, and the Effect of Modification with Myristic Acid and Biphenyl-4-Carboxylic Acid

-Nanobioengineering-

Master Thesis

Rasmus Müller Smedt and Tin Duy Nguyen

Aalborg University
Nanotechnology



Nanotechnology
Aalborg University
<http://www.aau.dk>

AALBORG UNIVERSITY

STUDENT REPORT

Title:

Characterisation of Model Peptides QKFFFDQ and QDFFFKQ, and the Effect of Modification with Myristic Acid and Biphenyl-4-Carboxylic Acid

Theme:

Nanobioengineering

Project Period:

2018-2019

Project Group:

5.321

Participants:

Rasmus Müller Smedt
Tin Duy Nguyen

Supervisors:

Peter Fojan

Copies: 0

Page Numbers: 49

Date of Completion:

June 10th 2019

Abstract:

Synthetic modification of peptides has gained interest as a way of mitigating the drawbacks of peptide-based drugs, such as the high metabolism of these compounds. The peptides QDFFFKQ and QKFFFDQ, based on the model peptide RFFFR, have been confirmed to fibrillate in polar solvents. The peptides were successfully modified with myristic acid and biphenyl-4-carboxylic acid by *in situ* carboxylic acid esterification as an extension of standard solid phase peptide synthesis. Circular dichroism and fluorescence measurements indicate that the peptides are stabilised by π -stacking. AFM measurements show a significant increase in fibrillation propensity for both peptides after modification with myristic acid or biphenyl-4-carboxylic acid. The significant decrease in solubility in aqueous environments after modification could prove detrimental for use in pharmaceuticals. As such, less hydrophobic moieties should be investigated.

Contents

Abbreviations	vii
1 Introduction	1
1.1 Peptidedesign	2
1.2 Simulation	4
1.2.1 Coarse Graining	5
1.3 Solid-Phase Peptide Synthesis	6
1.4 Lipidation	10
1.4.1 N-Terminal Lipidation Using Fmoc Based SPPS	10
1.5 Reverse Phased High-Pressure Liquid Chromotography	12
1.6 Thin Layer Chromotography	12
1.7 Mass Spectrometry	12
1.7.1 Circular Dichroism	13
1.8 Fluorescence Spectrometry	15
1.8.1 Protein Fluorescence	15
1.8.2 Energy Transfer	16
1.9 Atomic Force Microscopy	17
2 Materials and Methods	21
2.1 Materials	21
2.2 Methods	22
2.2.1 Simulation	22
2.2.2 Synthesis	22
2.2.3 HPLC	22
2.2.4 MS	23
2.2.5 TLC	23
2.2.6 CD	23
2.2.7 Fluorescence spectroscopy	23
2.2.8 AFM	23
3 Results and Discussion	25
3.1 Molecular Dynamics Simulations	25
3.2 HPLC	27

3.3	MS	30
3.4	TLC	32
3.5	CD	33
3.6	Fluorescence	37
3.7	AFM	41
4	Conclusion	49
	Bibliography	51
A		55
A.1	AFM	55

Abbreviations

AFM	Atomic force microscopy
Arg	Arginine
Asp	Aspartic acid
Boc	<i>tert</i> -butoxycarbonyl
CD	Circular dichroism
CG	Coarse-grained
DCC	N,N'-Dicyclohexylcarbodiimide
DCM	Dichloromethane
DIC	N,N'-Diisopropylcarbodiimide
DIEA	N,N-Diisopropylethylamine
DMF	N,N-Dimethylformamide
Fmoc	Fluoren-9-ylmethoxycarbonyl
FRET	Förster resonance energy transfer
Gln	Glutamine
HBTU	(2-(1H-benzotriazol-1-yl)-1,1,3,3-tetramethyluronium hexafluorophosphate
HCCA	α -Cyano-4-hydroxycinnamic acid
HOAt	1-Hydroxy-7-azabenzotriazole
HOBt	Hydroxybenzotriazole
LJ	Lennard Jones
Lys	Lysine
MD	Molecular dynamics
MS	Mass spectrometry
Oxyma	ethyl 2-cyano-2-(hydroxyimino)acetate
PET	Photoinduced energy transfer
Phe	Phenylalanine
SA	Sinapinic acid
SPPS	Solid phase peptide synthesis
TFA	Trifluoroacetic acid
THAP	2,4,6-Trihydroxyacetophenone
TOF	Time of flight

Chapter 1

Introduction

Peptides play an integral role in many biological processes and have shown great potential in pharmaceuticals due to their potential for high efficacy and minimal side effects. Additionally, due to significant advances in recombinant DNA technology, solid-phase peptide synthesis and purification technology, peptides are now generally considered a lead compound in drug development. As of 2013, 67 peptides are on the global market for clinical application, while around 270 are in clinical phases and over 400 are in advanced preclinical trials. Peptide-based drugs already exist for a variety of different diseases like osteoporosis, diabetes, hypothyroidism and even bacterial infections. Despite these advantages, peptide-based drugs have some major drawbacks, including rapid metabolism and poor permeation across some biological barriers, such as the blood-brain barrier. However, these drawbacks can be improved by synthetic modifications of the peptides.[1]

Lipidation of proteins is a common post-translational modification found in many natural biological settings[2]. In pharmaceuticals, lipidation has been shown to increase the circulation time of proteins and peptides in the bloodstream, thus increasing the therapeutic efficacy of such lipidated biomolecular compounds[3, 4, 5]. However, due to the hydrophobic nature of lipids, lipidation of a soluble peptide or protein will inevitably have an effect on the properties of the peptide or protein[6, 7]. It can cause unfolding of proteins followed by aggregation or fibrillation[2], most likely leading to reduced activity[8, 9].

Another area of research that has received considerable attention, is hydrogels based on fibrillar peptide networks[10]. While amyloid fibrillation has been associated with several diseases, including Alzheimer's disease and Parkinson's disease, nonpathogenic amyloid structures have also been discovered[11]. Peptide hydrogels show great potential for biomedical applications, such as tissue engineering[12, 13], drug delivery platforms[14] and cell culture scaffolds[15], due to their inherent biocompatibility[16].

In this study, the effects of different modifications on the supramolecular structure of fibrillating peptides QDFFFKQ and QKFFFDQ is investigated using circular dichroism, fluorescence and atomic force microscopy. The modification is performed

using a simple extension of the peptide synthesis.

1.1 Peptidedesign

Before designing a fibrillating peptide, it is important to know and understand the different interactions leading to fibrillation. Boden et al. have established some criteria for rational design of fibrillating peptides. First, fibrillation requires cross-strand attractive forces, which mostly depends on the side-chains of the amino acids making up the peptide. These forces include hydrophobic interactions, electrostatic forces, hydrogen bonding, and in more recent years π -stacking interactions have been found to help stabilise fibres[17]. These forces should also be sufficient in compensating for the translational and conformational entropies lost due to being locked in β -sheet formation. Second, for tapering to occur, there should be some lateral recognition between β -sheets build into the peptides to enforce anti-parallel tape-like structures and constrain their growth to one dimension. Third, it should be designed to have a certain solubility in the desired solvent, so that the fibrillation can be controlled.[18] Boden et al. have also produced a model of how fibres are formed at higher peptide concentrations as seen in figure 1.1.[19]

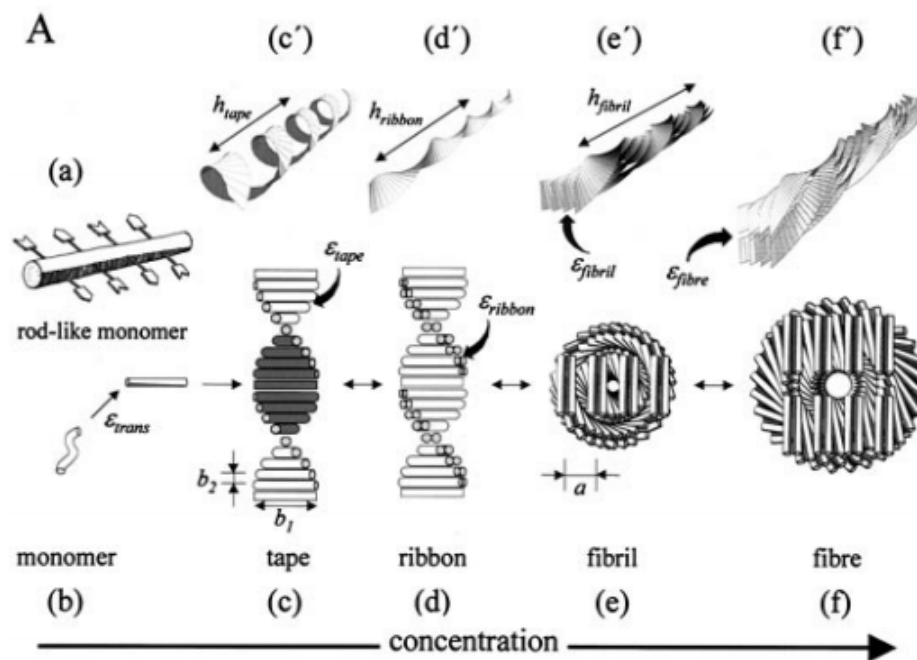


Figure 1.1: A model of the hierarchical self-assembly of chiral rod-like units. Local arrangements (c-f) and corresponding global equilibrium conformations (c'-f').

In this study, 2 peptides have been synthesised: QKFFFDQ and QDFFFKQ. Two different N-terminal modifications were performed on each peptide resulting in 6

different peptides. The two modifications of interest are the addition of a hydrophobic tail (myristic acid), and the addition of more aromatic rings (biphenyl-4-carboxylic acid). The peptides and their respective modifications can be seen in figure 1.2

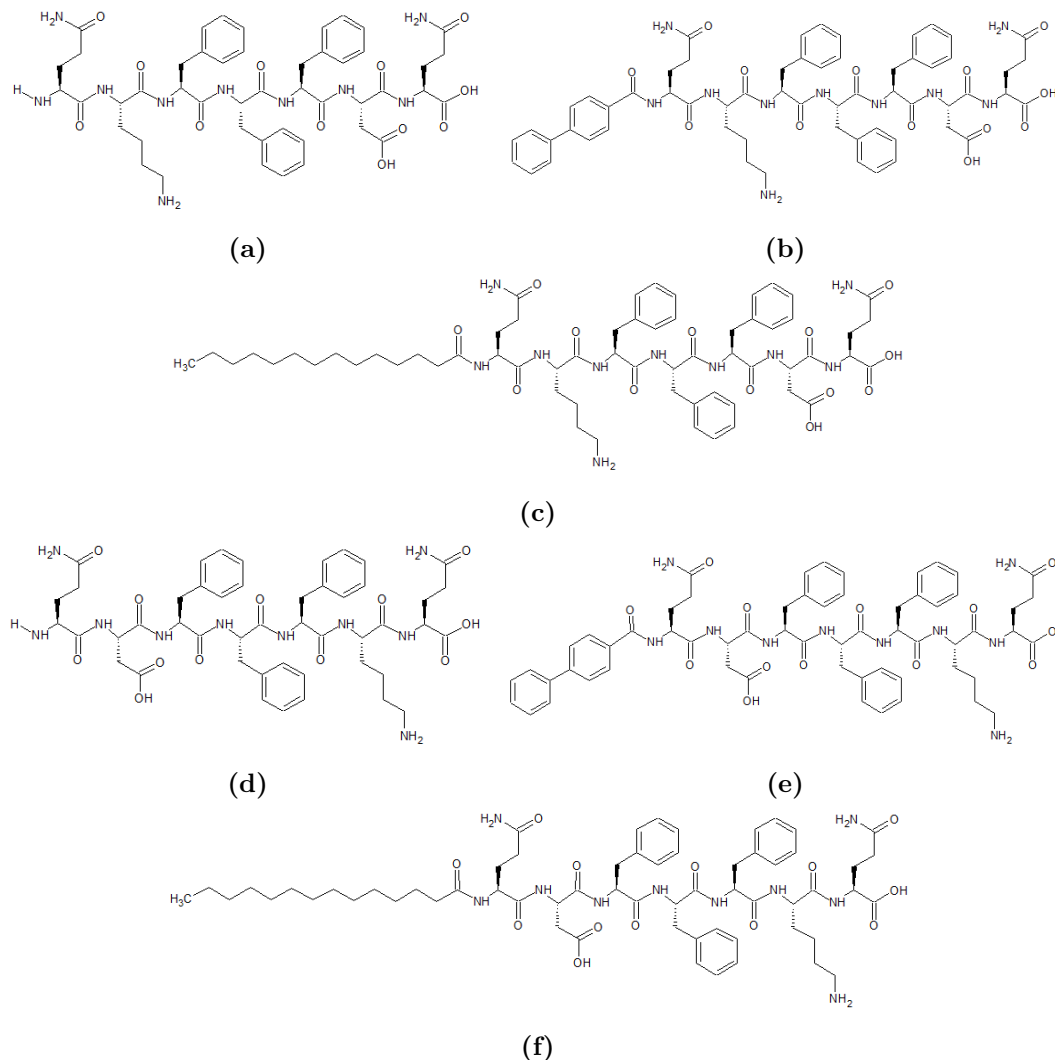


Figure 1.2: Structures of the different peptides synthesised in this study (a) QKFFFDQ (b) QKFFFDQ modified with biphenyl-4-carboxylic acid (c) QKFFFDQ modified with myristic acid (d) QDFFFKQ (e) QDFFFKQ modified with biphenyl-4-carboxylic acid (f) QDFFFKQ modified with myristic acid. Images were made using ChemSketch freeware.

The design of QKFFFDQ and QDFFFKQ is based on the triphenylalanine motif of the RFFFR peptide designed by Slyngborg et al., which is based on the LVFFA peptide derived from β -amyloid peptide[17]. Triphenylalanine allows for more π -stacking, thus increasing attractive forces between strands. Arg has been added at the ends of the peptide to lessen interaction between tapes, encouraging one-

dimensional growth. The fibrillation of RFFFR has already been characterised by Slyngborg et al.[20]. QKFFFDQ and QDFFFKQ utilise the same triphenylalanine motif as RFFFR, however, the Arg residues at the ends have been substituted for Asp and Lys, giving the peptide a neutral net charge, while also facilitating anti-parallel β -sheet formation. In addition to the oppositely charged amino acids, Gln was added at the ends, as later simulations of a KKFFFDD peptide found that the opposite charged ends could cause end to end interactions between strands limiting fibre growth, seen in figure 3.2 in section 3.1.

1.2 Simulation

Molecular dynamics (MD) is a simulation of movements of molecules or atoms, defined by their trajectories and position in a fixed time. Whether or not the movements are allowed is defined by classical mechanics, more specific Newtons equations of motion. This is used to equilibrate a system. The particles are spherical and can interact with each other, either by repelling when the particles are in close range or attraction at long range. The best-defined potential for both properties is the Lennard Jones (LJ) potential. LJ describes two particles interacting within a certain cutoff distance, r_c . The potential energy, u , for particles at position i and j , is given by:

$$u(r_{ij}) = \begin{cases} 4\epsilon \left[\left(\frac{\sigma}{r_{ij}} \right)^{12} - \left(\frac{\sigma}{r_{ij}} \right)^6 \right] & r_{ij} < r_c \\ 0 & r_{ij} \geq r_c \end{cases} \quad (1.1)$$

Where ϵ is the strength of the interaction and σ is the distance where the potential is zero.[21]

The environment the atoms are interacting in is usually a box, with certain boundary conditions. When simulating the particles in the box, the walls of the box does not interact with the particles at all but rather, when a particle reaches the boundary of the box, it reappears in the opposite side of the box. Thus, the whole system is treated as multiple boxes placed adjacent to each other. This is called periodic boundaries. The problem is that the particles close to the wall will interact with the particles in the adjacent box. To compensate for that the interaction range of particle is limited to only half of the box size.

When starting a simulation, initial conditions must first be set. The particle's position is set in a simple cubic lattice with a giving distance, whereby a velocity is given in an arbitrary direction. The magnitude of the velocity is dependent on the starting temperature. The temperature is not constant and fluctuates between 5-10%.

Additionally, the size of the box, number of particles, time step and starting temperature must be set. The initial position of the particles is set, ensuring they do not overlap each other. Normally a cubic lattice structure should be sufficient. The initial temperature is chosen such that, the lattice structure will melt and the particles are free to move upon starting the simulation. The velocity is given after

the positions have been set such that the sum of momenta in the system is zero. The simulation is not continuous and is instead divided into time steps. The position of a particle in a new time step is based on the current and previous positions, as well as the force acting on the particle.

Calculating the force of the particles acting on each other is very time consuming, so some simplification is made. An example is that particles force will only be considered if the distance between them is less than the cutoff distance as explained above. When the particles are close enough to interact LJ is used to calculate the force and potential energy. After this is done, the motion equation is integrated, to find the positions in which the particles are placed in the next time step. An example could be using the Verlet algorithm to determine the next position. The Verlet algorithm is derived from Taylor expansion:

$$r(t + \delta t) = r(t) + v(t)\delta t + \frac{1}{2}a(t)\delta t^2 + \dots \quad (1.2)$$

Where r is the position, v is the velocity and a is the acceleration. Deriving the Verlet algorithm one must look at both direction, as follows

$$\begin{aligned} r(t + \delta t) &= r(t) + v(t)\delta t + \frac{1}{2}a(t)\delta t^2 + \frac{1}{6}b(t)\delta t^3 + \mathcal{O}(\delta t^4) \\ r(t - \delta t) &= r(t) - v(t)\delta t + \frac{1}{2}a(t)\delta t^2 - \frac{1}{6}b(t)\delta t^3 + \mathcal{O}(\delta t^4) \end{aligned} \quad (1.3)$$

Then summation gives the Verlet algorithm

$$r(t + \delta t) = 2r(t) - r(t - \delta t) + a(t)\delta t^2 + \mathcal{O}(\delta t^4) \quad (1.4)$$

This means that the Verlet algorithm uses the position of the current and previous time step, to determine the new position. Using the Verlet does not require much computational power, but it also means that the precision is moderate, with an error of δt^4 . If the new position is accepted the loop repeats until the desired time steps are taken.[22]

1.2.1 Coarse Graining

One way of reducing the computational power needed for simulation is by using a coarse-grained (CG) model instead of simulating atomistic models. CG groups multiple atoms in the molecule into a single bead, thus simplifying the system. One CG model is the Martini force field, in which four non-hydrogen atoms are grouped into one CG bead. However, for smaller molecules with a ring structure, two non-hydrogen atoms are grouped into a bead. Figure 1.3 shows CG mapping of common compounds.

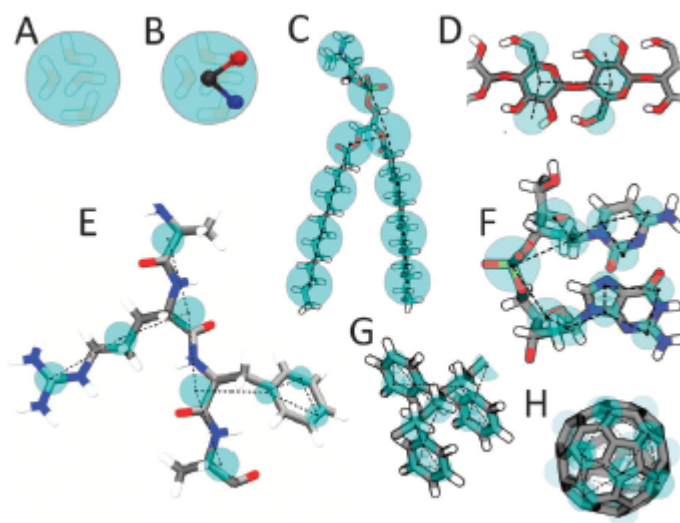


Figure 1.3: CG mapping (cyan beads) of A, water, B, polarizable water, C, DMPC lipid, D Polysaccharide, E peptide, F DNA fragment, G polystyrene fragment and H Fullerene. [23]

This means that simulation can be done in a larger timescale. The martini force field classifies the beads as one of 4 types; polar, non-polar, apolar and charged beads. Each of these types is divided again by their hydrogen bonding interactions, or by polarity.[23]

1.3 Solid-Phase Peptide Synthesis

Solid-phase peptide synthesis (SPPS) is a highly efficient technique for synthesising peptides and small proteins. In SPPS the first amino acid is anchored to a solid support or a matrix. The peptide then undergoes repeated cycles of deprotection, activation and coupling, each cycle adding another amino acid to the sequence. Finally, the peptide is released from the matrix and fully deprotected (usually done in the same step). SPPS is done by anchoring the C-terminus of the first amino acid to the matrix while having the N-terminus protected. The N-terminus is then deprotected and coupled with the activated C-terminus of new amino acid, thus growing the peptide from the N-terminus. The basic principle of SPPS is illustrated in figure 1.4.[24]

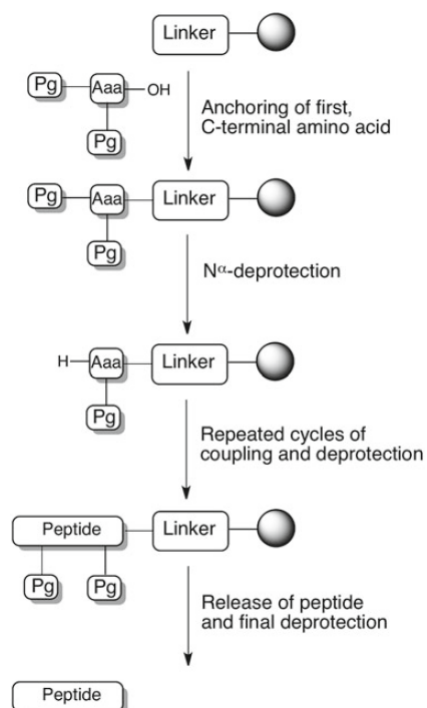


Figure 1.4: The principle of solid-phase peptide synthesis (SPPS).[24]

The overall strategy for SPPS is defined by the $N\alpha$ -protection group, the most common being flouren-9-ylmethyloxycarbonyl (Fmoc) and *tert*-butoxycarbonyl (Boc), as the protection group sets a window for possible chemical options. In the case of Fmoc, piperidine is used. Deprotection of Fmoc using piperidine is illustrated in figure 1.5.[24]

After the N-terminus is deprotected, it can react with an activated carboxylic acid of new amino acid. Activation is done by reaction with an electrophile, usually in conjunction with a nucleophile in order to avoid epimerisation. Frequently used electrophiles include DIC, DCC and HBTU. HBTU being an electrophile with a built-in nucleophile. Nucleophiles include HOBt, HOAt and more recently Oxyma. A list of common coupling reagents can be seen in figure 1.6. [24]

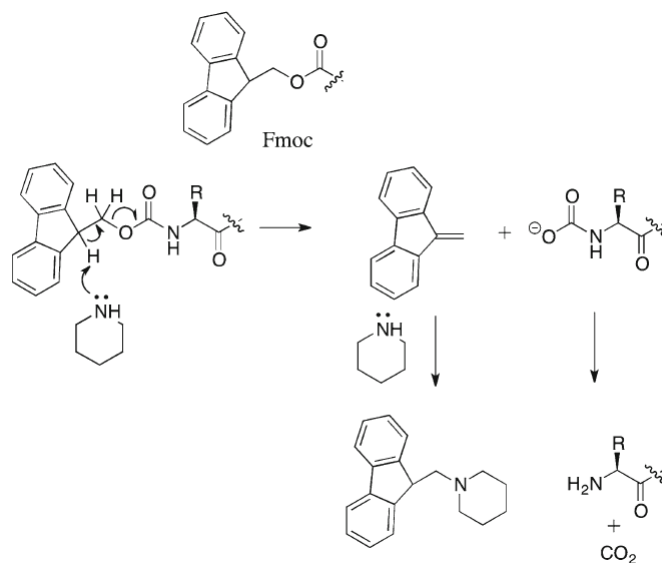


Figure 1.5: Deprotection of Fmoc using piperidine as base and nucleophilic scavenger.[24]

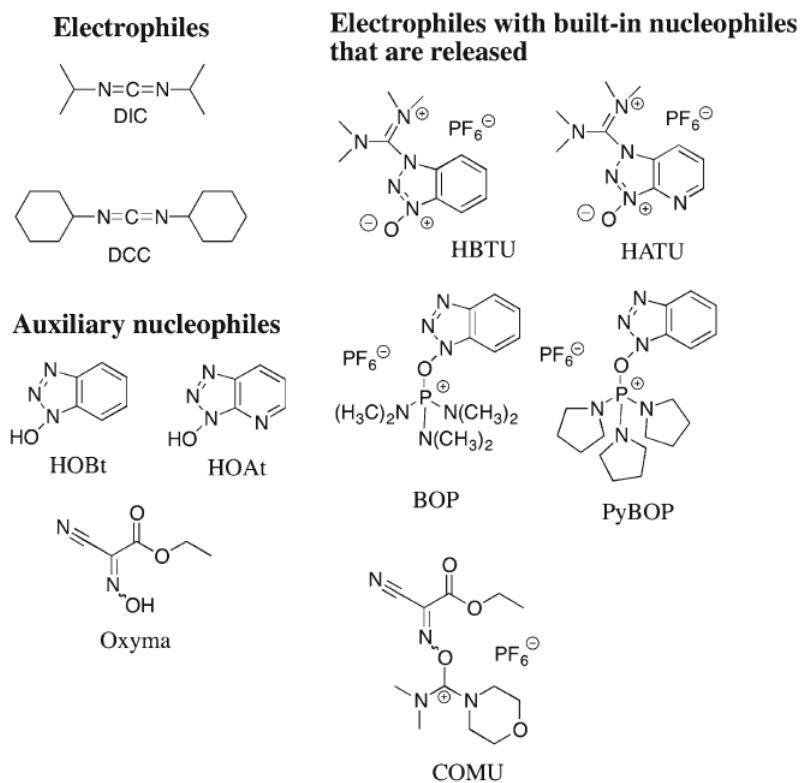


Figure 1.6: Some common electrophiles and nucleophiles.[24]

The electrophile used in this paper is HBTU. DIEA is used to activate the carboxylic acid group of the incoming amino acid, which then reacts with HBTU to form an activated ester. The activated amino acid can then react with the N-terminus of the linked peptide. The specific coupling chemistry of HBTU is illustrated in figure 1.7 and 1.8.[24]

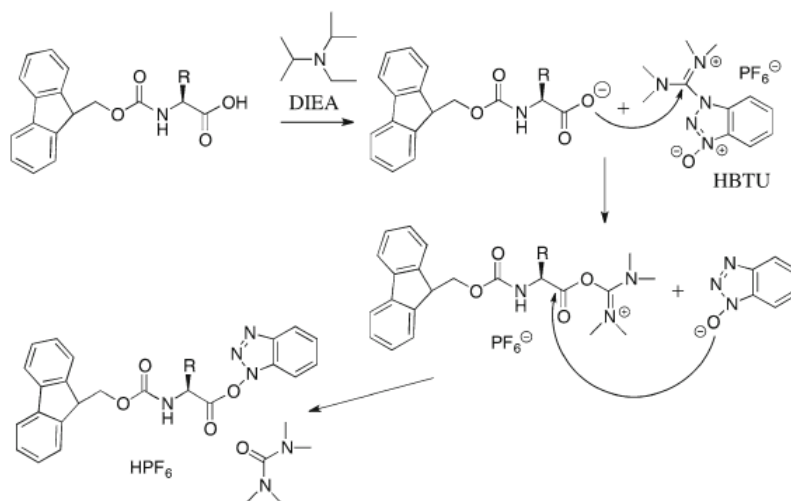


Figure 1.7: Formation of activated ester using HBTU.[24]

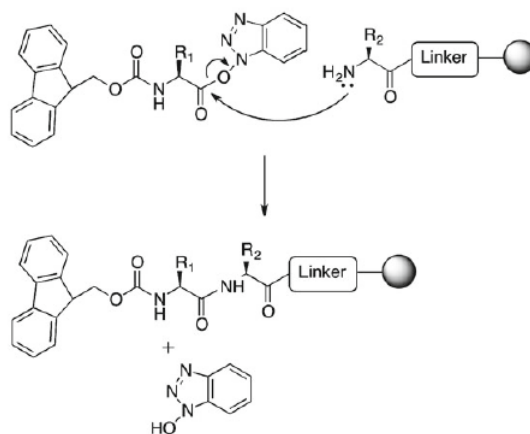


Figure 1.8: Coupling of HBTU activated ester to peptidyl-resin.[24]

Once the full peptide chain has been synthesised, it needs to be split from the resin and fully deprotected. This is done by acidolysis, typically with TFA, as most resins swell well in TFA. Additionally, TFA is volatile and easily evaporated. The most common side chain protection groups are also TFA labile, and can thus be removed in the same step. One side effect of this is that the removal of side chain

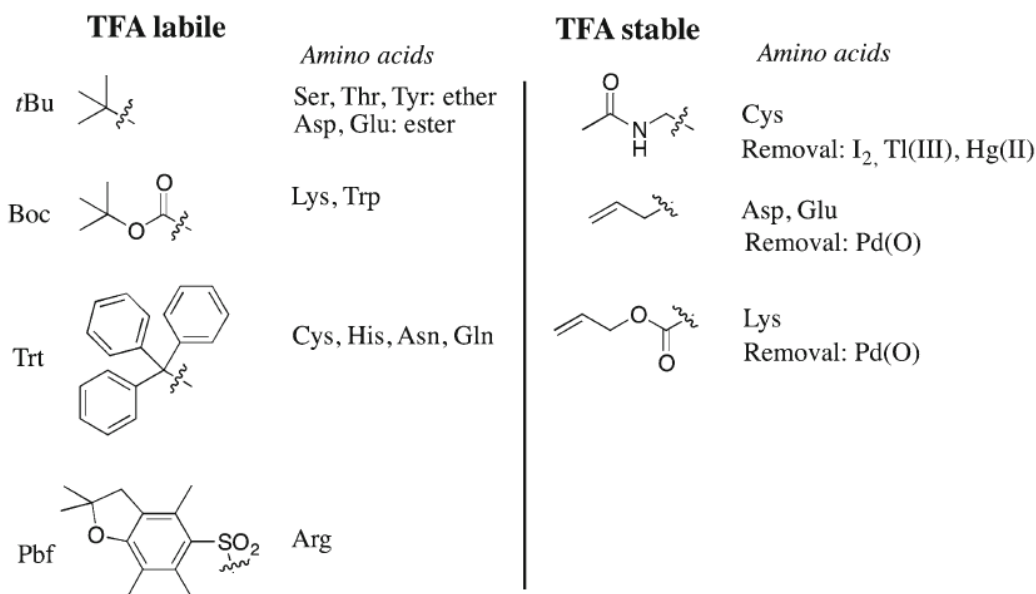


Figure 1.9: Common side-chain protecting groups used in Fmoc-SPPS. Protecting groups on the left are removed with TFA, while the protecting groups on the right are not.[24]

protection groups can generate carbocations which can cause side reactions. As such, nucleophilic scavengers, such as water and TIS, is usually added to the splitting solution. Common side chain protecting groups can be seen in figure 1.9.[24]

A linker or handle is used to anchor the peptide to the resin. The linker should have the characteristics of a protection group in order to allow peptide growth while being able to release the finished peptide under well-defined conditions. In the case of Wang linkers, an N α -protected amino acid is attached to the linker via esterification, which can then be deprotected and coupled as usual. The peptide can then be released using TFA, making Wang linkers ideal in conjunction with TFA labile side chain protection groups.[24]

1.4 Lipidation

Lipidation is a broad term for the covalent attachment of lipid molecules to a protein or peptide. Lipidation is a common post-translational modification found in many natural biological settings, one example being N-terminal glycine myristoylation. N-terminal glycine myristoylation is the attachment of a saturated myristic acyl group called myristoyl to the N-terminal glycine of a protein using an amide bond.[25]

1.4.1 N-Terminal Lipidation Using Fmoc Based SPPS

N-terminal lipidation can be done as an extension of normal SPPS. This requires a fully functional peptide head-group to be synthesised before the hydrophobic tail-

group can be attached. The tail-group can either be coupled directly as an activated compound or by forming an active ester *in situ* using traditional SPPS reactions.[26]

In figure 1.10, an activated lipophilic tail compound is attached to a finished peptide, by first deprotecting the N-terminus using piperidine, then adding the active compound. The peptide complex is then fully deprotected and released from the resin using TFA.[26]

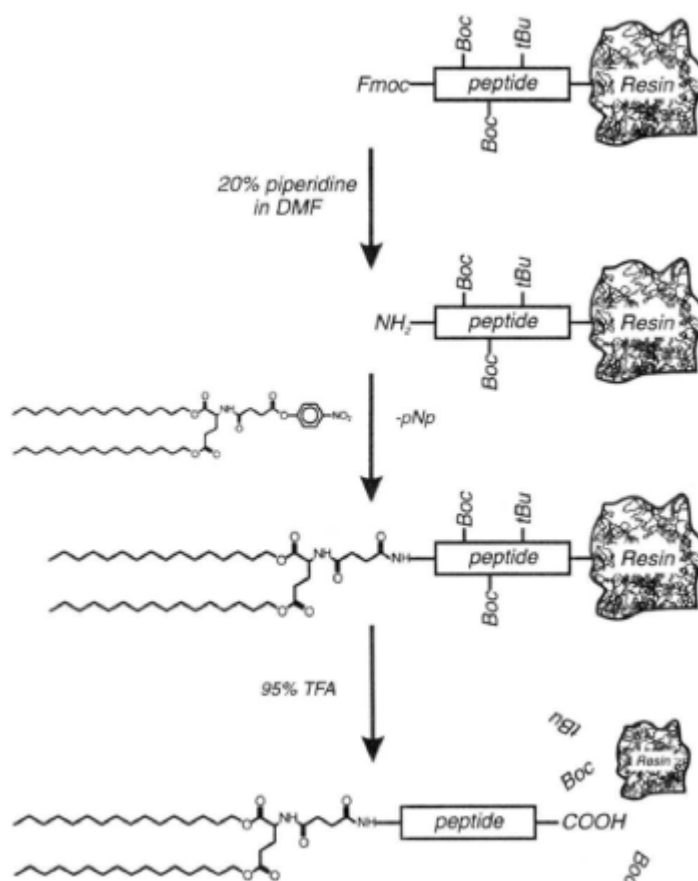


Figure 1.10: Elongation of peptide with a lipophilic tail.[26]

In this paper, myristic acid and Biphenyl-4-carboxylic acid is attached to a finished peptide by *in situ* activation. The process is similar to the HBTU activation described previously and thus requires the lipid to have a carboxylic acid group. The activation and coupling of biphenyl-4-carboxylic and myristic acid follows the same mechanism as shown in figure 1.7 and 1.8.

1.5 Reverse Phased High-Pressure Liquid Chromotography

Reverse phased high-pressure liquid chromatography (RP-HPLC), is a method generally used to analyse a sample. In order to analyse the sample, it needs to be dissolved in an aqueous polar mobile phase and injected into a hydrophobic column. The column is the stationary phase, which normally consists of hydrophobic alkyl chains that will interact with the hydrophobic parts of the sample. The length of the alkyl chains depends on which sample is being analysed, as short alkyl chains, C4, is used for capturing big molecules like proteins, and long chains, C18, is used for smaller molecules like peptides. An organic mobile phase is injected in a gradient concentration, which separates the sample over time. UV or fluorescent detectors are used to detect the sample, yielding a graph of absorption over retention time. Different sizes of columns are also available depending on if the sample needs to be collected or analysed. A small column is used for analysing a sample, while a larger preparative column is used when collecting and purifying a sample.[27]

1.6 Thin Layer Chromotography

Thin layer chromatography (TLC), is a separation method used for analysing contents of a sample. A sample of dissolved solute is deposited on a thin layer of sorbent on a plate (stationary phase). The plate is then placed in a container with a small amount of solvent (mobile phase), which is absorbed by the sorbent. As the solvent reaches the solute on the plate, it will draw it across the plate. The different compounds in the solute will separate depending on properties like polarity, size or adsorption.[27]

Usually, the TLC plate needs to be visualised, which is done by staining the plate with a detection reagent. The most widely used detection reagent for peptides and proteins is ninhydrin, which gives a pink, yellow or violet colour after reaction with amides and amino acids. The retardation factor can then be calculated, which is the ratio of how far the solute has moved compared to the total distance the mobile phase has moved.[28]

1.7 Mass Spectrometry

Mass spectrometry (MS) is a method in which molecules are ionised and separated based on mass. Ions are created from atoms or molecules by impact with an electron from an ion source. The energy from the electron is transferred and an electron from the molecule is ejected. This molecule is then a molecular ion and travels through a spectrometer that separates the molecules by mass to charge ratio.

There are many ways to ionise a molecule, which depends on the size and structural composition of the material. Some examples could be Electron impact ionisa-

tion (EI) where electrons are passed through a sample that is in the gas phase, which then generates molecular ions where the molecule remains intact, or fragmented ions, where the molecule is fragmented by collision with an electron. This is mostly used for small molecules below 1kDa, as larger molecules will fragment more, making it difficult to analyse the compound. If larger molecules of up to 200kDa need to be analysed, electrospray ionisation (ESI) could be used. In ESI a solution of the sample is sprayed across a high potential difference, however, the sample needs to be charged for this to work. Another ionisation method is the Matrix-assisted laser desorption/ionisation (MALDI) which is used in this study, as it is non-volatile to the sample, and works for large molecules below 500kDa. MALDI is a method that uses a sample matrix mixture, which is applied on a surface and left to crystallise. An infrared or ultraviolet laser, then irradiate the surface, and the matrix absorbs the energy and ionise the sample.[29]

The laser is focused on a small spot of sample-matrix, and pulses thousands of shots, causing the sample-matrix to evaporate and ionise. Several types of matrices can be used, some common ones being THAP, SA and HCCA. Figure 1.11 shows the structure of the matrix.

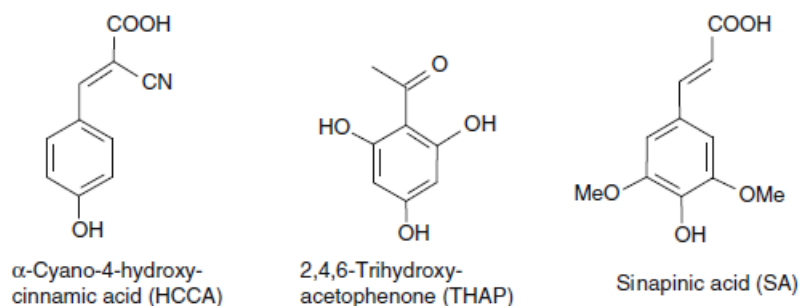


Figure 1.11: Structure of MALDI matrices. [29]

Once more the size of the analyte determine which matrix is best suited. For nucleotides smaller than 3.5kDa THAP is used. For peptides and small proteins of less than 10kDa, HCCA is used, while for peptides and proteins larger than 10kDa, SA is used. The detection method used in this study is time of flight (TOF). TOF is a method in which ions that have the same kinetic energy moves with different velocity because of the differences in mass. These ions travel in a path of a given length and the detector measures the mass to charge ratio.[29]

1.7.1 Circular Dichroism

Circular dichroism (CD) is a method in which circular polarised light is emitted on a sample, which then absorbs either left or right polarised light in a non-equal ratio. This results in an elliptical polarisation, which is then measured. For CD to happen,

the molecule needs to have a chiral centre. In the case of amino acids in peptides and proteins, the amino acid has a chiral centre at the C_α , with the exception of glycine. Aromatic ring side-group in the residue absorbs in the near UV spectrum, while in the amide group in the backbone is absorbing in the far UV spectrum. Thus, conformational changes in the peptides and proteins can be observed in this spectrum. The secondary structures have characteristic spectra, which can be seen in figure 1.12.[30]

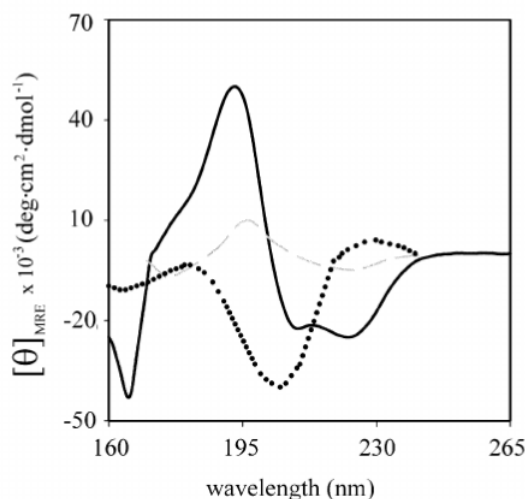


Figure 1.12: CD spectra of myoglobin, α -helix(-), β -sheet, concavalin(- -), and polyproline-II-type (...). [30]

α -helix has a negative peak at 222nm and 208nm, and a positive peak at 190nm. β -sheet, gives a negative peak is at 215nm and a positive peak at 195nm. It is important to note that the β -sheet structure shows more variety compared to the α -helix structure, which leads to variations in the signal peaks. Additionally, in the range between 225-235nm, the β -signal will be inhibited by the aromatic side-group in the residue, making the signal less accurate.[30] While the ellipticity is determined by the conformation of the peptide, concentration and cell path length also affect it. In order to take these factors into consideration, the molar ellipticity is used instead. The molar ellipticity can be calculated using the following equation:

$$\theta_{molar} = \frac{\theta_\lambda * M}{10 * d * c} \quad (1.5)$$

Where θ_λ is the observed ellipticity in mdeg, M is the molecular weight in g/mol, d is the path-length in cm and c is the concentration in g/L.[31]

1.8 Fluorescence Spectrometry

Fluorescence is the emission of light from a fluorophore due to relaxation from a higher excitation state. When light of a certain wavelength is emitted onto a fluorophore, containing aromatic structures, the electrons get excited, which then emits photons upon relaxation to the ground state.

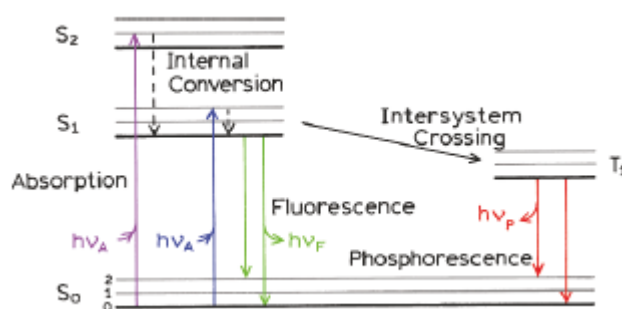


Figure 1.13: An example of a simple Jablonski diagram.[32]

When light is used to excite the fluorophore, the fluorophore absorbs the light, which makes the electron jump from the ground state, S_0 , to the excited electronic state, S_1 or S_2 , as seen in Figure 1.13. In each of these states, the electron can be at a number of vibrational energy levels, denoted 0, 1, 2. The electron loses some energy due to internal conversion (for example heat) then returns to the ground state, emitting fluorescence. The excitation and emission wavelength are usually not the same due to internal energy conversion. Molecules can also undergo spin conversion from an excited state to a triplet state, T_1 , which leads to phosphorescence.[32]

1.8.1 Protein Fluorescence

Fluorescence can be used on biomolecules containing aromatic rings, such as peptides or proteins.

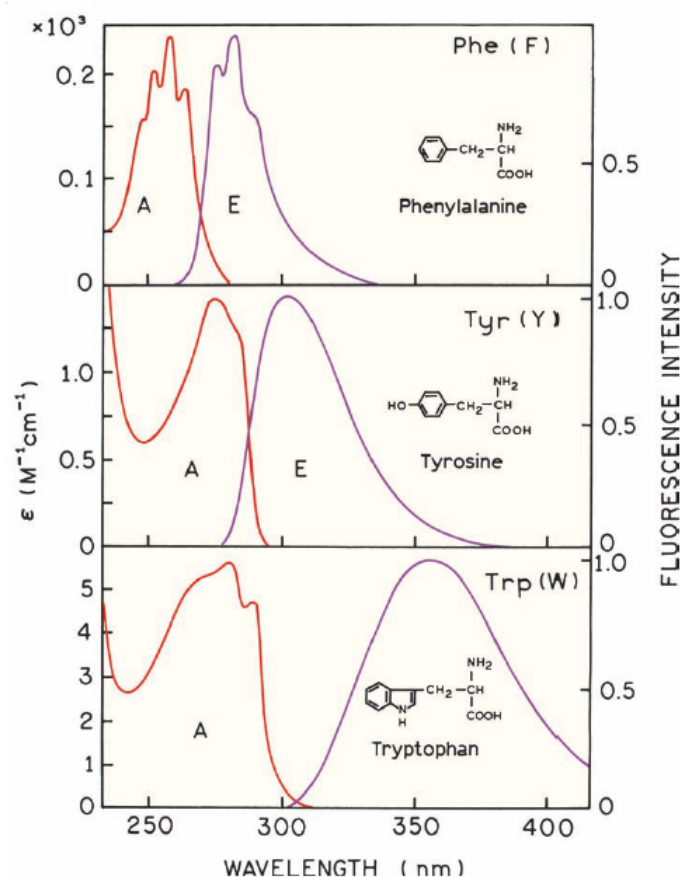


Figure 1.14: Absorption and emission spectra of Phenylalanine, Tyrosine and Tryptophan.[32]

Figure 1.14 shows the absorption and emission of aromatic amino acids. Phe has the shortest absorption and emission wavelength with an emission maximum at 282 nm, Tyr at 303 nm and Trp at 350 nm. The excitation wavelength should be around the absorption peaks of the respective aromatic amino acids. The fluorescent intensity of Phe, Tyr and Trp depend on the quantum yield, which is the number of emitted photons relative the number of absorbed photons. Phe has a quantum yield of 0.03, Tyr of 0.13 and Trp of 0.14. The emission of the aromatic rings are sensitive to local change in environment, conformational change, denaturing and binding.[32]

1.8.2 Energy Transfer

The fluorophore can also interact with the solvent, causing a change in intensity due to energy transfer. This is called quenching. Förster Resonance energy transfer (FRET) and photoinduced electron transfer (PET) are two mechanisms of energy transfer and depend on the distance between fluorophore and quencher. While FRET has a decrease in intensity of r^6 in the nanometer range, PET happens in Van Der

Waal domain, which is in the subnanometer range. When the distance between two fluorophores is so small, the overall electron distribution changes causing a red-shift in absorption spectrum.[33]

1.9 Atomic Force Microscopy

Atomic force microscopy (AFM) is a technique that can measure surface structure with an unprecedented resolution of down to 5nm image sizes. It works by physically scanning the sample with a small probe, measuring the deflection of the probe and building a topographic image of the sample.[34]

The general setup of an AFM consists of a laser, cantilever (with tip), position-sensitive photodetector, electronics and a sample, as illustrated in figure 1.15. As the surface is scanned, the cantilever deflects and the deflection is detected by the photodetector.[35]

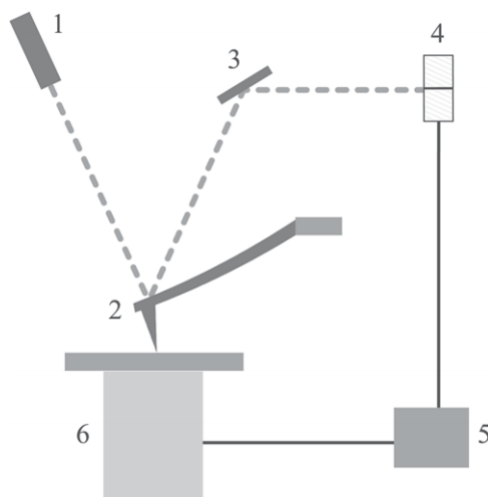


Figure 1.15: Illustration of a basic AFM setup consisting of 1 laser diode, 2 cantilever with tip, 3 mirror, 4 position sensitive photodetector, 5 electronics, 6 scanner with sample.[35]

The essential parameters for image resolution are the sharpness of the tip apex, measured by the radius of curvature, and the aspect ratio of the tip as a whole, as seen in figure 1.16.[35]

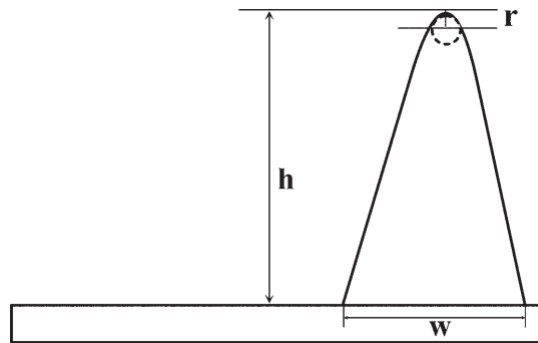


Figure 1.16: The essential parameters of the tip, radius of curvature (r) and aspect ratio (ratio of h to w).[35]

The AFM utilises a feedback loop so that it not only measures the forces but controls them by adjusting the cantilever. When a deflection of the cantilever is measured by the photodetector, highly precise piezoelectric elements move the probe or sample up or down, so that the deflection is reset.[34, 35]

The images are formed by measuring the effects of the close-range interaction forces between the cantilever tip and the sample surface. AFM utilises an LJ potential illustrated in figure 1.17.[35]

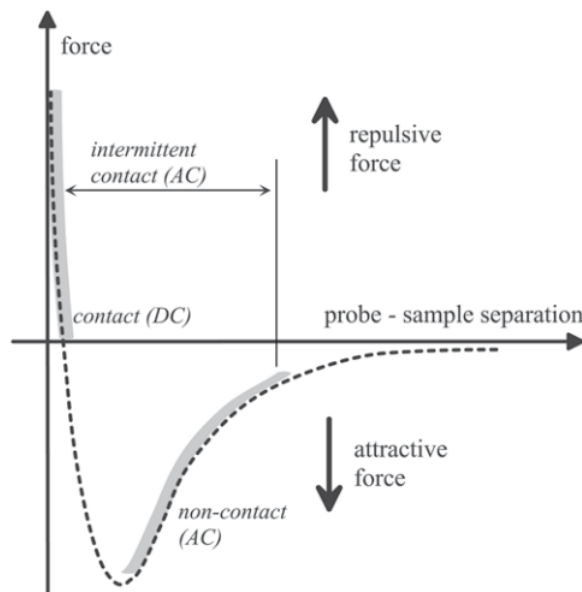


Figure 1.17: The LJ potential plot of the forces between tip and sample, highlighting where the general imaging modes are operative.[35]

The 3 general modes of running AFM are contact mode, non-contact mode and

intermittent contact mode. Contact mode measures the close range repulsive forces of the surface by putting the tip into contact with the sample. In contact mode, the force is kept constant by the feedback loop. As the tip is in constant contact with the sample, there is an increased risk of damage to the tip or sample when running contact mode. Non-contact mode mitigates this by having no contact between tip and sample. The cantilever is instead kept oscillating a short distance away from the sample. The short-range attractive forces of the sample induce a shift in the resonance peak of the cantilever, which is used to operate the feedback loop. While the vertical resolution is good, the lateral resolution is lower than other operating modes. Intermittent contact mode is similar to non-contact, however, the oscillating tip is brought into contact with the sample. When the distance between probe and sample is decreased, the oscillation is dampened and the feedback loop is operated by keeping the oscillation amplitude constant. Intermittent contact mode is the most common operating mode, as the lateral and vertical resolutions are good while minimising the contact between tip and sample. The operation of the different modes are illustrated in figure 1.18.[35]

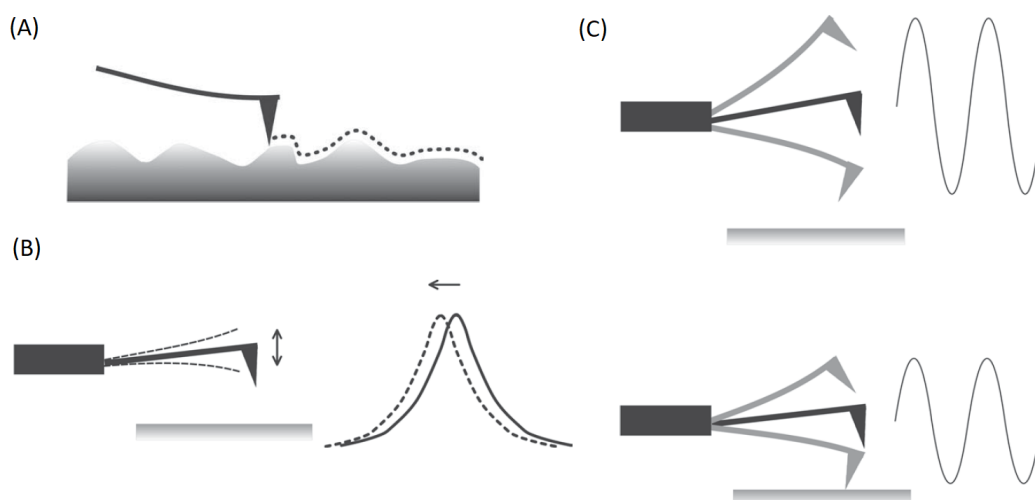


Figure 1.18: Illustrations of different operation modes of AFM. In contact mode (A) the tip directly follows the topography of the sample. The force is kept constant. In non-contact mode (B) the tip oscillates and the attractive forces induce a shift in resonance peak. Resonance phase is kept constant. In intermittent contact mode (C) the tip also oscillates but is brought into contact with the sample dampening the oscillation amplitude. The amplitude is kept constant.[35]

Chapter 2

Materials and Methods

2.1 Materials

Table 2.1: Chemical List

Chemicals	Cas	Description	Supplier
Fmoc-L-Phe-OH	35661-40-6		Matrix Innovation
Fmoc-L-Gln(Trt)-Wang resin	FL-200-0601		Matrix Innovation
Fmoc-Lys	71989-26-9		Matrix Innovation
Fmoc-Gln	132327-80-1		Matrix Innovation
Fmoc-Asp	71989-14-5		Matrix Innovation
Myristic acid	544-63-8		Sigma Aldrich
DMF	68-12-2	Lot# 122595G	Iris Biotech GmbH
DCM	75-09-2		Iris Biotech GmbH
Piperidine	110-89-4		Iris Biotech GmbH
DIEA	7087-68-5		Sigma Aldrich
Oxyrna	3849-21-6		Iris Biotech GmbH
HBTU	94790-37-1		Iris Biotech GmbH
TFA	76-05-1		Iris Biotech GmbH
TIS	6485-79-6		Iris Biotech GmbH
Acetonitrile	75-05-8		TH Geyer
PBS buffer		1x at pH 7.45	In house
Diethylether	60-29-7	Lot# V1I778141L	Iris Biotech GmbH
Ninhydrin	485-47-2		Honeywell Fluka
Methanol	67-56-1		Sigma Aldrich
Biphenyl-4-carboxylic acid	92-92-2		Sigma Aldrich
Ethanol	64-17-5		VWR BDH Chemicals

2.2 Methods

2.2.1 Simulation

The peptides are created atomistically in YASARA, then converted to coarse-grained (CG) 1:4 mapping with the martinize.py v2.6 script. Gromacs v5.1.2[36] was used for MD simulation. A box of 7x5x5 nm was generated with 13 nmol of the peptide inserted at random. Afterwards, the system was solvated with polarised martini water, followed by energy minimisation with Martini v2.2P force field[37, 38]. Finally, a 200ns MD simulation was run, with a time step of 20fs. The final clusters were visualised using VMD v.1.9.4a12[39] and the peptide backbones were visualised using the Bendix v1.1 extension.[40]

2.2.2 Synthesis

Synthesis was done by SPPS using ActivoSyn. The machine was cleaned before doing a synthesis. Afterwards, the reactor chamber with the Wang resin was loaded into the machine along with the Fmoc protected amino acid in Greiner tubes. 0.5M HBTU/0.5M Oxyma and 1M DIEA in DMF was used for activation, while 25% piperidine in DMF was used for deprotection. Finally, DCM was used to wash DMF from the reaction chamber.

Splitting

Splitting was done by adding 4 mL of 95% TFA, 2.5% miliQ water and 2.5% TIS in the reactor chamber and loading it into the ActivoSyn P12. The splitting program was set to shake the reaction chamber for 45min. After splitting was done, the peptide solution was collected in a 50mL Greiner tube and filled halfway with Diethyl ether. It was then centrifuged at 6000rpm at 4°C for 10min. Afterwards, the pellet was kept, while the supernatant was discarded. The pellet was resuspended with diethyl ether and centrifuged again. This process was repeated 3 times in total. After the final centrifugation, the pellet was left in a fume hood to dry overnight.

2.2.3 HPLC

The analyte was prepared by dissolving 0.001mg/mL of the peptide in 5% acetonitrile in milliQ water. The sample was sonicated for 30min or until all peptide was dissolved. 0.04mL was then injected in the Ultimate 3000 HPLC machine. The flow in the mobile phase has been set to 1.5mL/min. The protocol takes 96min per run and the absorbtion was measured at a wavelength of 214nm. The program used was Chromeleon. The column was Jupiter 5U C16 analytik 300 A.

2.2.4 MS

The analyte was prepared by dissolving 10mg/ml of the matrix HCCA in 0.1% TFA in 70% acetonitrile in water. Then 0.5 μ L of the matrix solution was mixed with 0.5 μ L of the sample on a target plate. The mixture was left to crystallise, after which the target plate was put in the MALDI-TOF apparatus. Each spot was shot in 1000 pulses 5 times while collecting all data.

2.2.5 TLC

The analyte was prepared by dissolving peptides in 70% Acetonitrile. The mobile phase used was a mixture of Acetonitrile, Methanol and MilliQ water at a ratio of 65:25:4. Samples were deposited 1cm from the bottom of a silica gel aluminium plate by using 2-3 μ L capillary pipettes. The TLC chamber was filled to roughly 0.5cm with the mobile phase and left to saturate for 30min with the lid closed. The plate was placed in the chamber and the lid was closed. When the mobile phase was 1cm from the top of the TLC plate the process was stopped.

Development of the TLC plates was done using 0.1g ninhydrin in 50mL ethanol. The ninhydrin solution was sprayed onto the TLC plate until soaked. Once dry, the TLC plate was heated using a hot plate at 90°C and then visualised with UV.

2.2.6 CD

The analyte was prepared by making a stock solution of 100 μ M. The stock was then immediately diluted to concentrations of 5, 10, 20, 50, and 75 μ M. PBS was used as the solvent for unmodified peptides, while 70% Acetonitrile in water was used as solvent for modified peptides. The measurements were done using a quartz cuvette with a 1cm path length. Parameters for the wavelength range was from 190nm to 260nm with a step of 1nm. Data were averaged over 8 consecutive measurements. The machine used was Jasco J-715, and the program used was Spectra Manager.

2.2.7 Fluorescence spectroscopy

The samples prepared for CD are re-used for fluorescence measurements. Measurements were done using a quartz cuvette with a path length of 1cm. The excitation wavelength was set to 250nm and the emission was measured in the spectrum from 260nm to 400nm. Before measurements were done, the intensity was checked to be between 2000-500000. If the intensity was not between 2000-500000, the aperture was adjusted until within this range. The spectrophotometer used was Chronos DFD ISS model 90021.

2.2.8 AFM

1x1 cm silicon wafers were cleaned by sonication in acetone for 30min, followed by treatment in a UV chamber for 30min.

Samples were prepared by dissolving $600\mu\text{M}$ peptide ($1000\mu\text{M}$ for biphenyl modified peptides) in 70% acetonitrile in water. $50\mu\text{L}$ of solution was deposited on the wafer and incubated for 30, 60 and 120min. After incubation, the wafer was rinsed carefully with water and the wafers were carefully dried using a nitrogen gun.

The AFM measurements were performed using NT-MDT Solver, operating in intermittent contact mode using the program Nova 1.1.1 Revision 14256. The cantilever used for measurements was silicon tip from ScanSens GmbH

AFM images were analysed using Gwyddion freeware[41].

Chapter 3

Results and Discussion

3.1 Molecular Dynamics Simulations

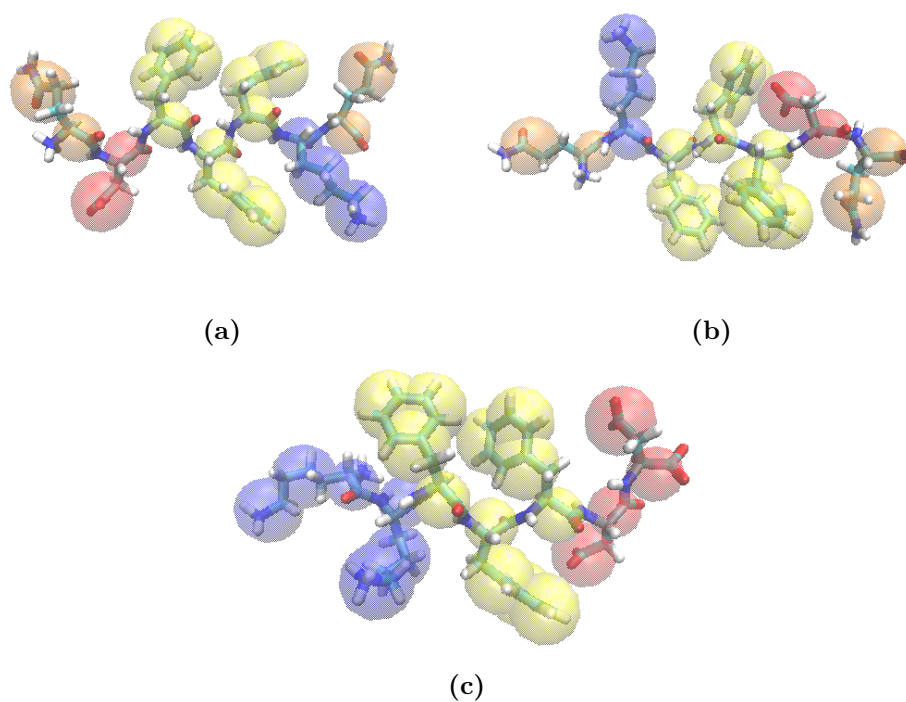


Figure 3.1: Coarse grained mapping (coloured beads) layered on top of atomistic structure (licorice representation) (a) QDFFFKQ (b) QKFFFDQ (c) KKFFFDQ. The coarse grained beads are colour coded by residue; Gln: Orange, Lys: Blue, Phe: Yellow and Asp: Red.

Atomistic structure of QDFFFKQ, QKFFFDQ and KKFFFDQ were coarse-grained, prior to MD simulations, in order to decrease computational load^{3.1}.

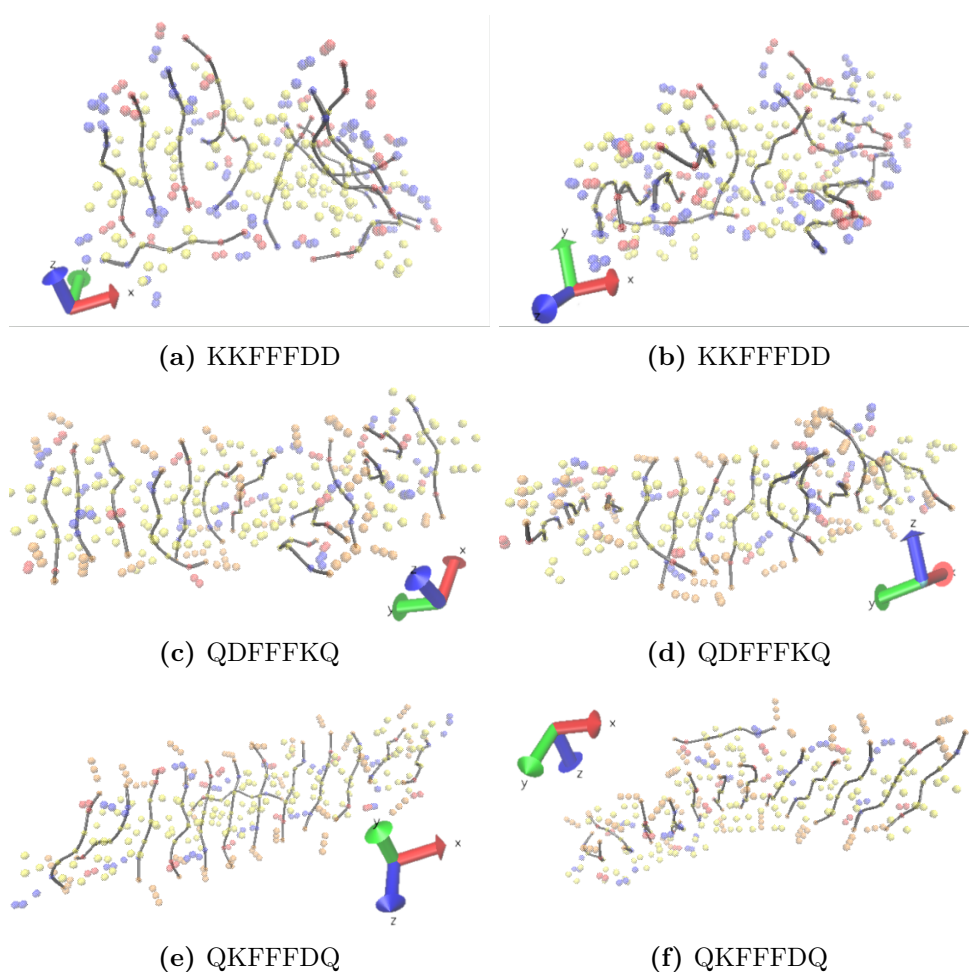


Figure 3.2: Snapshots of clusters of 13 peptide monomers after 200ns MD simulations at a temperature of 300K. (a, b) KKFFFDD, (c, d) QDFFFKQ, (e, f) QKFFFDQ. The side-chains are shown as transparent beads colour-coded by amino acids; Lys: blue, Phe: yellow, Asp: red, Gln: orange.

MD simulations of KKFFFDD (figure 3.2a and 3.2b) produced multiple partial anti-parallel β -sheets and not a single β -sheet tape. This could be due to the interactions between the charged amino acids at the ends not conforming to the rules of peptide fibrillation stipulated by Boden et al., specifically that the recognition between peptide monomers is not only lateral and thus the fibril growth is not limited to one direction[18]. In the MD simulations, this is seen as peptide monomers showing end to end interactions between β -sheets, ultimately leading to a relatively globular cluster.

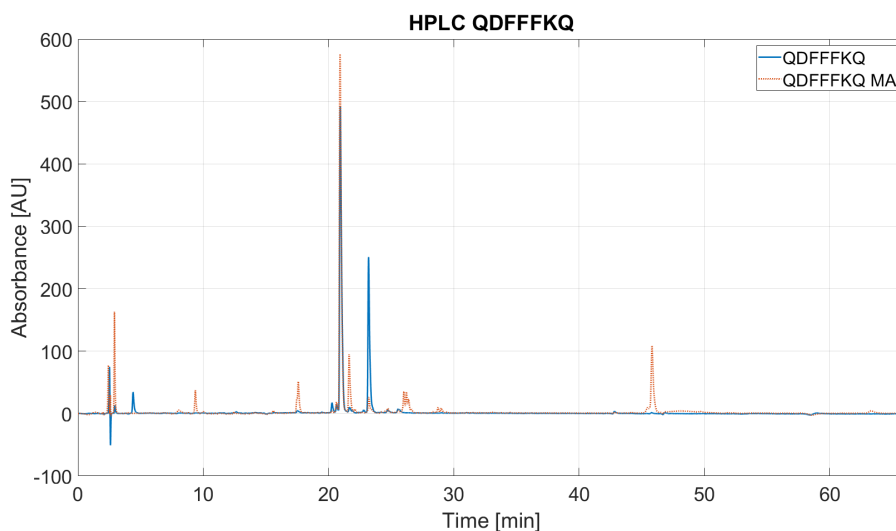
QDFFFKQ (figure 3.2c and 3.2d) produced anti-parallel β -sheets. It does not form a uniform tape, instead, it forms several fragmented β -sheet tapes. However, it is clear that the lateral recognition is increased compared to KKFFFDD.

QKFFFDQ (figure 3.2e and 3.2f) produced a highly ordered single tape. Only a single peptide monomer does not conform to the tape. This could be due to the

simulation box size being too small for all 13 peptides monomers to self-assemble into a single tape. A slight helicity can also be observed, which is expected for β -amyloid fibrils based on a triphenylalanine structure[20].

From these MD simulations, it is evident that substituting charged terminal amino acids with Gln removes the end to end interactions between peptide monomers, leaving only lateral interactions, thus enabling fibrillar growth. The difference between QDFFFKQ and QKFFFDQ could be explained by the orientation of the aromatic rings of Phe in relation to Lys and Asp as the coarse-grained Asp consists of an additional bead compared to coarse-grained Lys, as seen in figure 3.1. It should also be noted that, since the peptides are coarse-grained, these simulations are not ideal representations of the actual self-assembly. However, they still provide a good indication of the fibrillation potential of these peptides.

3.2 HPLC



(a)

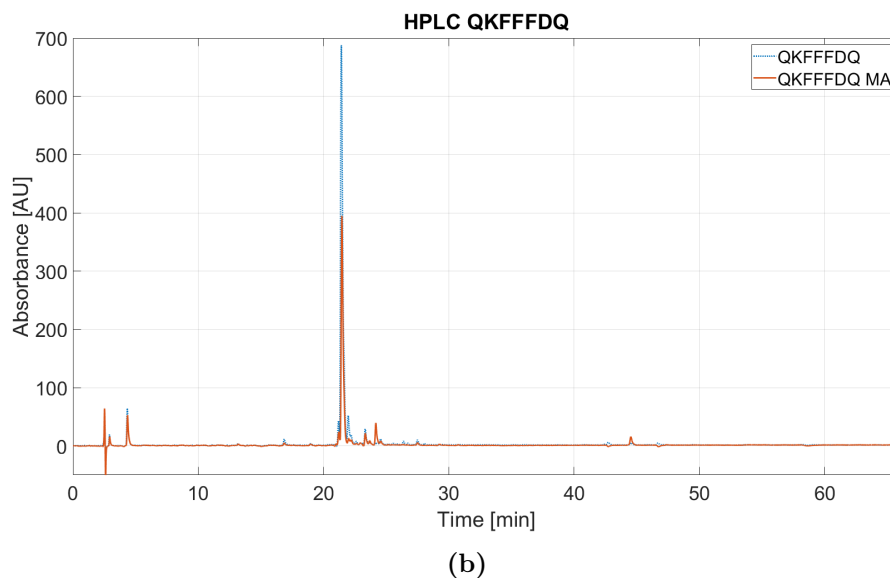
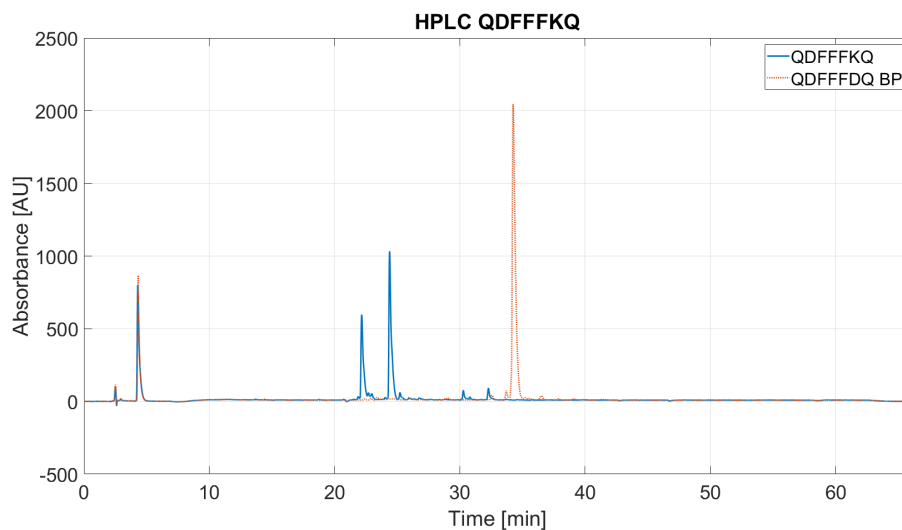


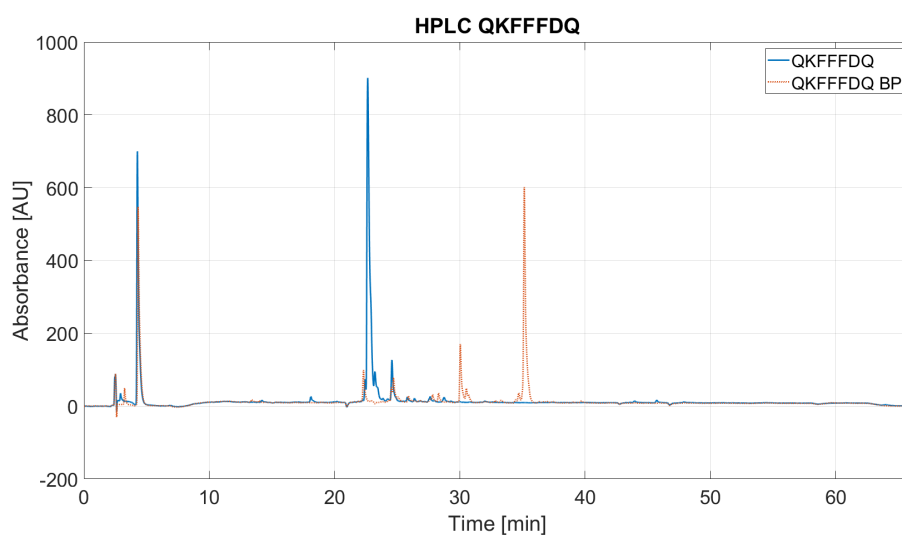
Figure 3.3: HPLC of unmodified peptides in blue and myristic acid modified peptide in orange (a) QDFFFKDQ and QDFFFKQ MA (b) QKFFFDQ and QKFFFDQ MA. The samples have been dissolved in 5% acetonitrile in water. The absorption is measured at a wavelength of 214nm and the flow is set to 1.5mL/min. The retention time is measured for 66min with a gradient of acetonitrile from 5-80%. An injection peak is observed after 4 min.

HPLC analysis shows an indication of successful modification of peptides with myristic acid (figure 3.3a and 3.3b). QDFFFKQ shows multiple significant peaks, meaning the sample is likely impure. The main peak of the modified peptides overlaps with the main peak of the unmodified peptides at 21min, indicating that a significant amount of peptide remains unmodified after synthesis with myristic acid. QDFFFKQ MA shows a small but considerable peak around 46min, which is expected as the modification with myristic acid should significantly increase the overall hydrophobicity of the peptide, increasing the retention time in the RP-HPLC column. QKFFFDQ MA shows a significantly smaller but noticeable peak at roughly the same time. This peak could also be an indication of successful modification of QKFFFDQ. It is notable that QDFFFKQ MA and QKFFFDQ MA could not be completely dissolved in the 5% acetonitrile solution, whereas QDFFFKQ and QKFFFDQ are easily dissolved in the 5% acetonitrile solution. As such, it is likely that all the unmodified peptide in the QDFFFKQ MA and QKFFFDQ MA sample was dissolved, while only a small amount of successfully modified peptide was dissolved. Thus the high peaks of QDFFFKQ MA and QKFFFDQ MA at 21min compared to the small peaks around 45min are not indicative of the actual ratio between modified and unmodified peptide in these samples. The reason for the lower success rate of myristic acid modification could be due to aggregating of the activated myristic acid ester, as early experiments with stearic acid showed considerable aggregation after esterification. Due to the low solubility of the modified peptides in

the mobile phase for HPLC, TLC was used to verify the successful modification of QDFFFKQ MA and QKFFFDQ MA. These results can be seen in section 3.4.



(a)



(b)

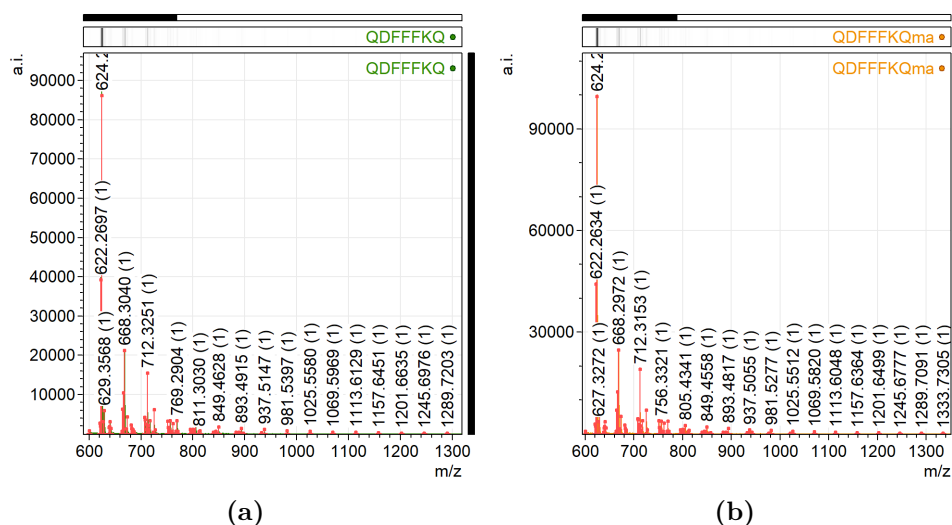
Figure 3.4: HPLC of unmodified peptides in blue and biphenyl modified peptide in orange (a) QDFFFKDQ and QDFFFKQ BP (b) QKFFFDQ and QKFFFDQ BP. The samples have been dissolved in 5% acetonitrile in water. The absorption is measured at a wavelength of 214nm and the flow is set to 1.5mL/min. The retention time is measured for 66min with a gradient of acetonitrile from 5-80%. An injection peak is observed after 4 min.

Figure 3.4a and 3.4b shows a clear separation between the main peaks of modified and unmodified peptide indicating that the modification was successful. The peaks

of QDFFFKQ BP and QKFFFDQ BP are in range 35-36min. QDFFFKQ still shows the same impurity observed in 3.3a. QKFFFDQ BP also shows impurity from the significant peak at 30min. A small peak from QKFFFDQ BP also overlaps with QKFFFDQ, however, this could be contamination from insufficient cleaning of the needle used for loading sample into the HPLC.

HPLC data indicate that modifications have been successful. However, figure 3.3a and 3.3b shows a significant amount of unmodified peptide in the QDFFFKQ MA and QKFFFDQ MA samples. Ideally, these samples should be purified for further experiments. However, the low solubility of QDFFFKQ MA and QKFFFDQ MA at low concentrations of acetonitrile made it impractical to use semi-prep HPLC to separate the unmodified peptide from the modified, as the high concentration of acetonitrile necessary to dissolve them, would simply cause the peptides to flush through the column. MS was used to verify the molecular structure with limited success, as seen in section 3.3. Additionally, as MS was not available for further experiments, it was not possible to use MS to determine which peaks belong to the synthesised peptides in the impure samples. As such, no further purification was performed, and all subsequent experiments were carried out using these samples.

3.3 MS



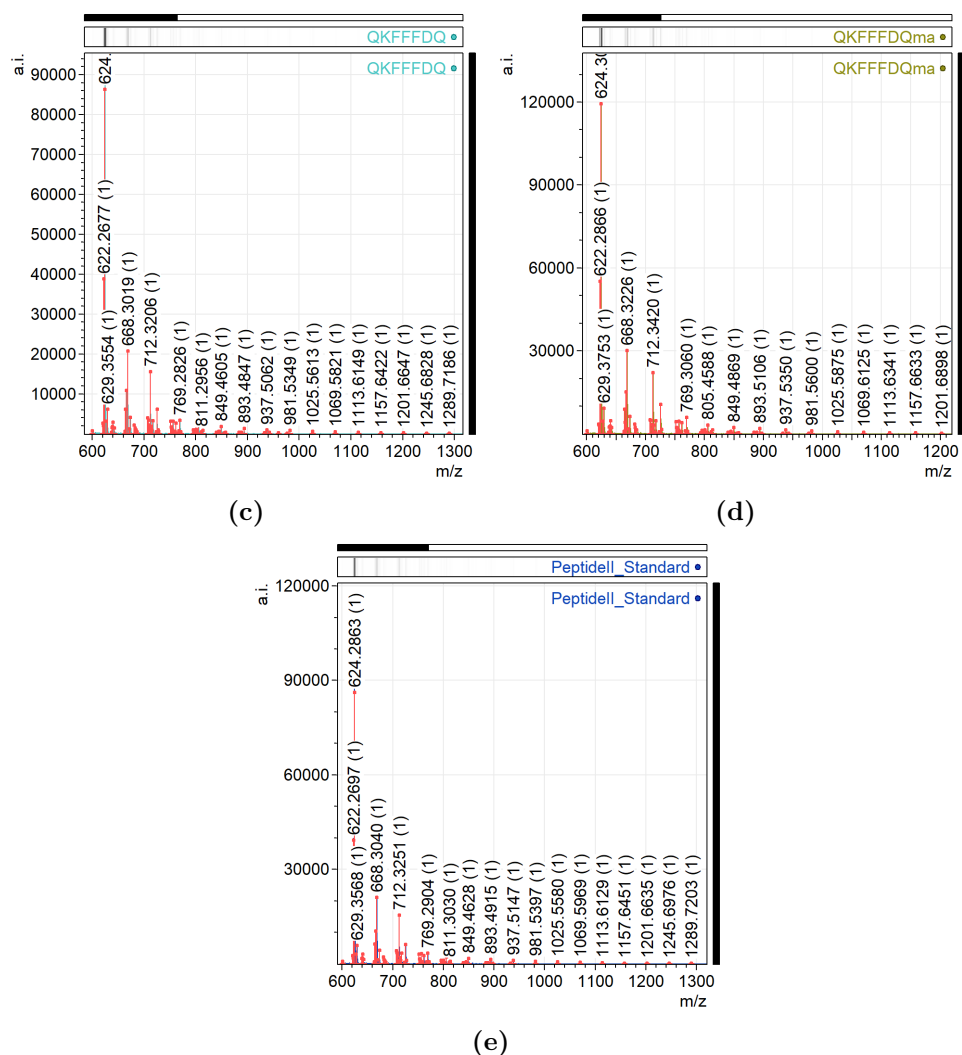


Figure 3.5: MALDI-TOF spectra of (a) QDFFFKQ, (b) QDFFFKQ MA, (c) QKFFFDQ, (d) QKFFFDQ MA and (e) Peptide standard II. The matrix used is HCCA and the concentration of the peptides is $1\mu\text{M}$ in 50% acetonitrile in water.

When looking at the MS data (figure 3.5) it is not possible to determine if the peptide is present, as QDFFFKQ and QKFFFDQ should have a m/z of 959.4676 u, while QDFFFKQ MA and QKFFFDQ MA should be 1170.6738 u. What is observed instead is that all spectra show the same peaks as the Peptide II standard used for calibration, meaning all the samples have possibly been mixed with Peptide standard II. It was not possible to redo the measurement, as the equipment and staff were not available.

3.4 TLC

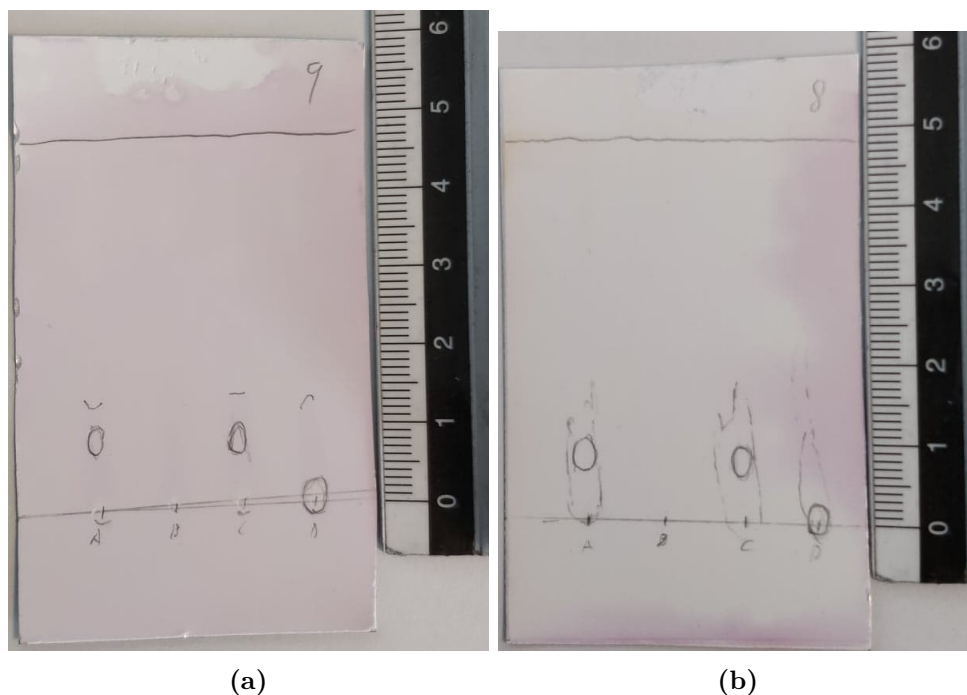


Figure 3.6: TLC of QDFFFKQ (a) and QKFFFDQ (b). Unmodified peptide in lane A, myristic acid in lane B, mix of the unmodified peptide and myristic acid in lane C and the modified peptide in lane D. The mobile phase is acetonitrile, methanol and water solution at a ratio of 65:25:4. Staining was done with ninhydrin and visualised with UV where the visual spots were marked with a pencil.

TLC was performed on QDFFFKQ MA and QKFFFDQ MA along with their respective unmodified variants to determine if the modification was successful (figure 3.6). Both peptides have been visualised with ninhydrin and UV light, where significant spots were marked. As ninhydrin only reacts with amino acids and amides, myristic acid cannot be visualised. The retardation factor, r_f , has been calculated for the visible spots inserted in table 3.1. This is done by taking the distance from the starting line to the centre of the spot and divided by the whole length.

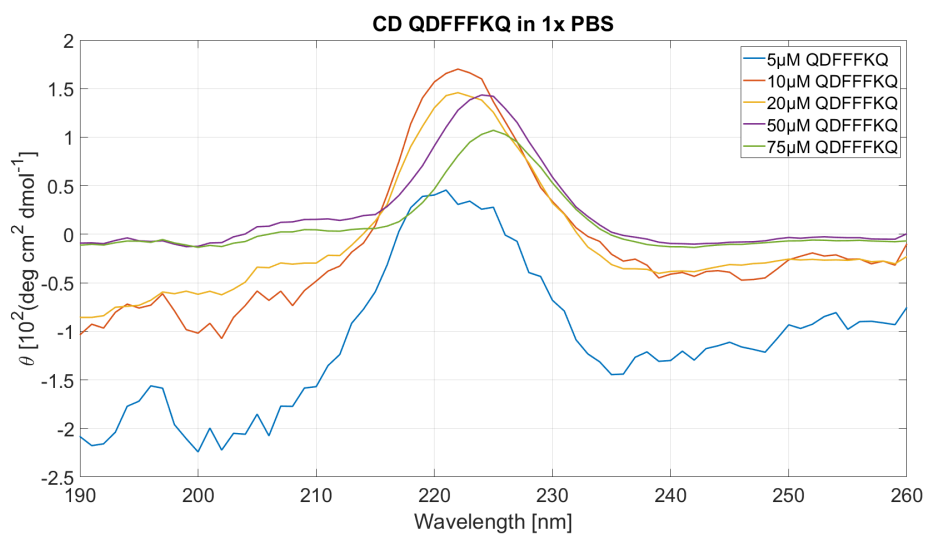
r_f	(A) Peptide	(C) Peptide & MA mix	(D) MA modified peptide
QDFFFKQ	0.190	0.190	0.019
QKFFFKQ	0.165	0.151	0.016

Table 3.1: Calculated r_f values

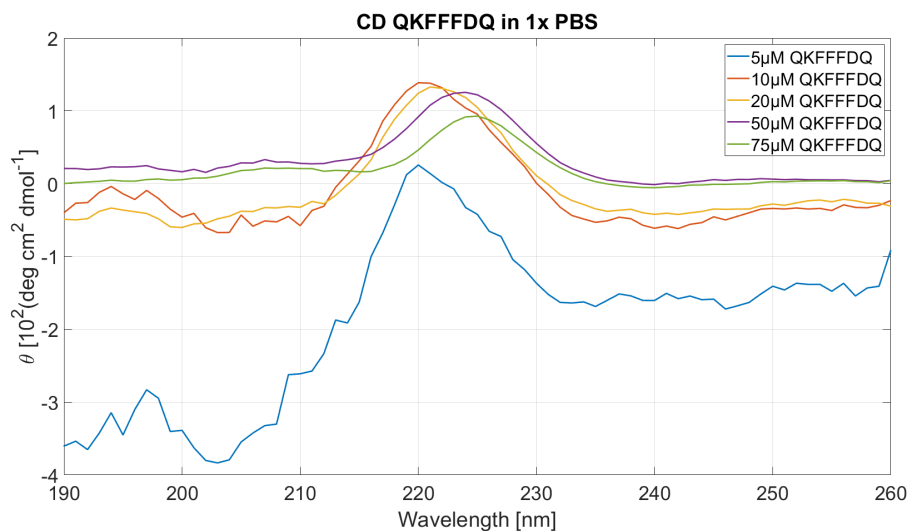
It is clear that the peptides in lane D were successfully modified, as the solute in lane D shows a r_f value of 0.019 and 0.016, which is much lower than lane A and C. In fact, the value is so low that it likely has not moved at all. The reason for

this is might be explained by QDFFFKQ MA and QKFFFDQ MA already forming supramolecular structures at low molarity in high concentrations of acetonitrile, as evident from CD and fluorescence measurements (figure 3.8 and 3.11 respectively). The lack of significant spots with r_f values of 0.150 to 0.190 in lane D does show that purity of QDFFFKQ MA and QKFFFDQ MA are significantly higher than what was observed in HPLC measurements (figure 3.3), as previously hypothesised.

3.5 CD



(a)



(b)

Figure 3.7: CD spectra of (a) QDKKKFQ and (b) QKFFFDQ, with a wavelength range of 190-260nm. The solutions were prepared by dilution from a stock solution of $100\mu\text{M}$ with 1x PBS. A quartz cuvette with a path length of 1cm was used.

CD spectra of QDFFFKQ and QKFFFDQ (Figure 3.7a and 3.7b) shows no signals indicating β -sheet structure, which could be due to the low solution concentration, the small size of peptides or the compact supramolecular structures formed by the peptides[17], as these are prone to cause artefacts in a CD spectra[42]. QDFFFKQ and QKFFFDQ both have a peak around 220nm at $5\mu\text{M}$ shifting towards 225nm at higher concentrations. Peaks in the range 220-230nm have previously been attributed to π -stacking for other short peptides with aromatic compounds[17, 43, 44, 45]. QDFFFKQ shows a clear shift between 20-50 μM , indicating a critical fibre concentration in this range. A similar shift is seen for QKFFFDQ, however not as pronounced. Concentrations of $5\mu\text{M}$ and below shows a high degree of noise, which is likely due to the noise being amplified when calculating molar ellipticity.

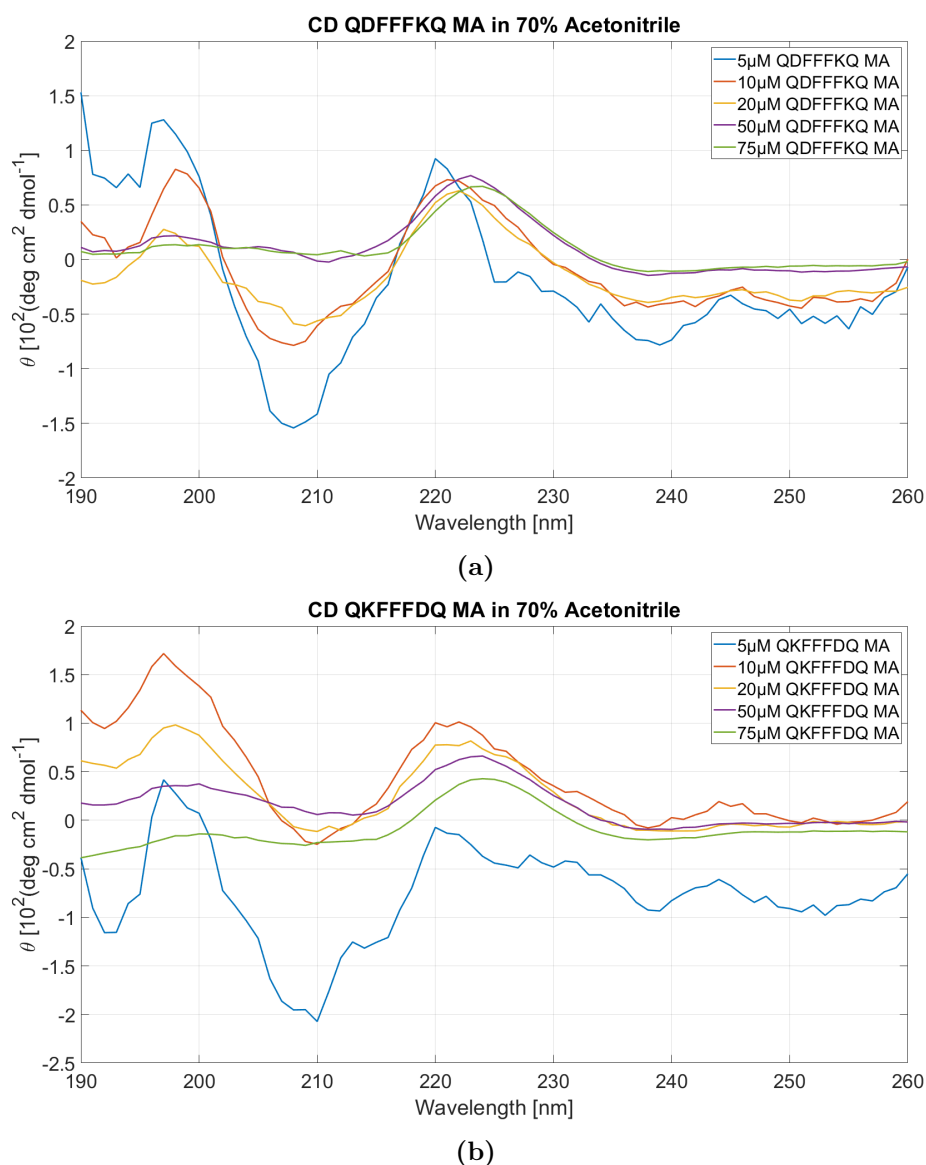


Figure 3.8: CD spectra of (a) QDKKKFQ MA and (b) QKFFFDQ MA, with a wavelength range of 190-260nm. The solutions were prepared by dilution from a stock solution of $100\mu\text{M}$ with 70% acetonitrile in water. A quartz cuvette with a path length of 1cm was used.

QDFFFKQ MA and QKFFFDQ MA (figure 3.8a and 3.8b) show a peak shift from 221nm to 224nm which is similar to the non-modified peptides. Furthermore, at low concentrations, a negative peak is observed for both peptides at 208-210nm with a positive peak at 197nm, which could indicate anti-parallel β -sheet formation[46]. Interestingly, this peak disappears at $50\mu\text{M}$ for both peptides. As previously mentioned, this is likely due to the peptides forming compact supramolecular structures, as the CD spectra begin to look similar to the CD spectra observed for the un-

modified QDFFFKQ and QKFFFDQ. The same is observed for QDFFFKQ BP and QKFFFDQ BP (figure 3.9a and 3.9b).

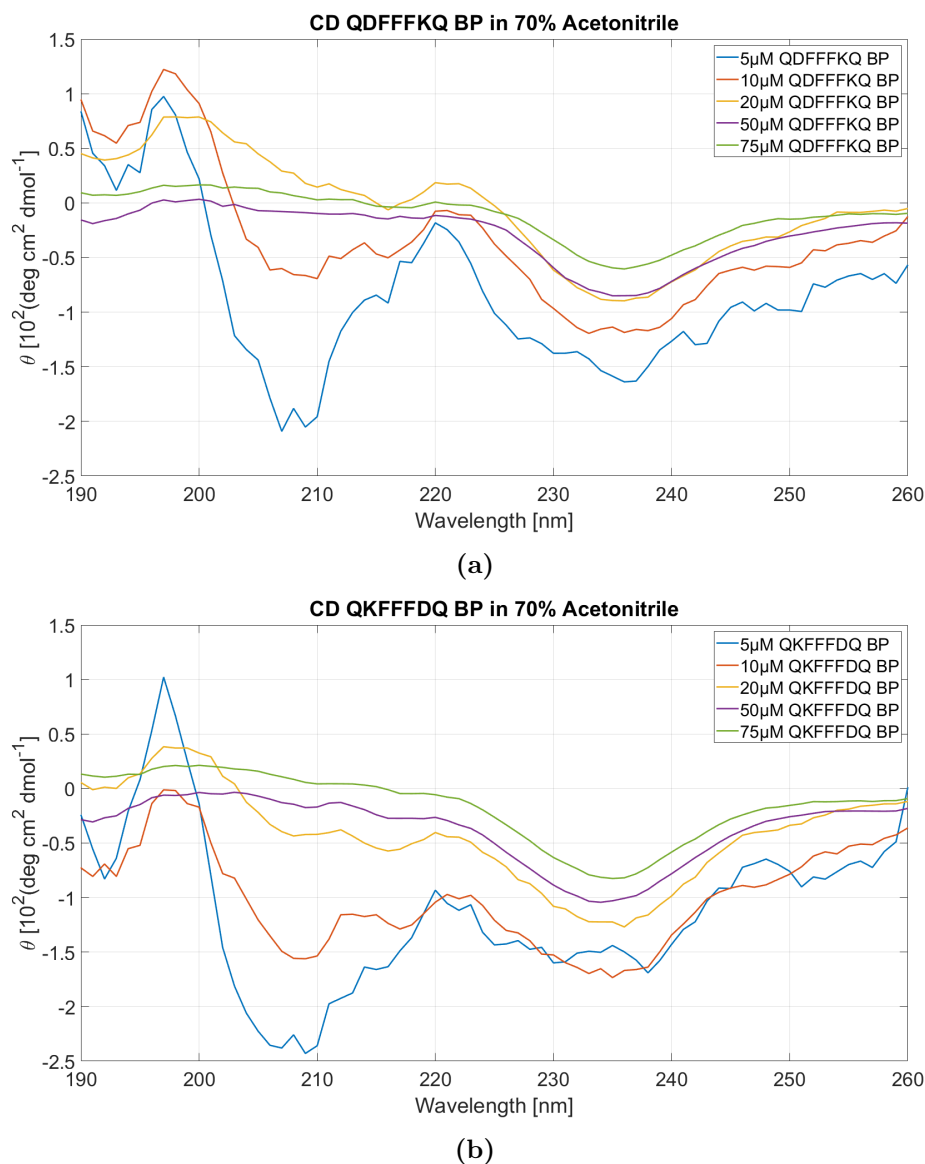


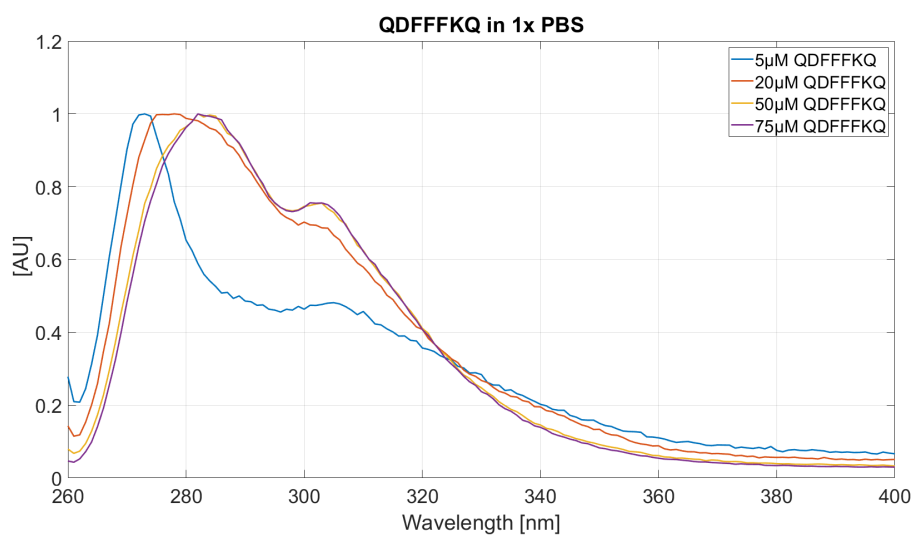
Figure 3.9: CD spectra of (a) QDFFFKQ BP and (b) QKFFFDQ BP, with a wavelength range of 190-260nm. The solutions were prepared by dilution from a stock solution of 100 μ M with 70% acetonitrile in water. A quartz cuvette with a path length of 1cm was used.

Unlike the other peptides, CD spectra of both QDFFFKQ BP and QKFFFDQ BP (figure 3.9a and 3.9b) show a negative peak around 235 nm. The specific origin of this peak is unknown, however, it could be due to the biphenyl moiety utilising a different π -stacking conformation than triphenylalanine. Previous MD simulations

of the RFFFR peptide designed by Slyngborg et al. showed that triphenylalanine formed T-shaped π -stacking[20]. However, the biphenyl moiety is likely forming either sandwich or parallel displaced π -stacking, resulting in a negative peak around 235nm. At low concentrations ($5\mu\text{M}$ - $20\mu\text{M}$) peaks around 221nm are observed, which is still indicative of π -stacking, as the large negative peak at 235nm would cause a peak at 226nm to blue-shift. The reason this peak disappears at higher concentrations could be due to the signal at 235nm drowning it out.

In general, CD spectra show indications of π -stacking in all samples, as well as anti-parallel β -sheets structure at low concentrations for QDFFFKQ MA, QKFFFDQ MA, QDFFFKQ BP and QKFFFDQ BP.

3.6 Fluorescence



(a)

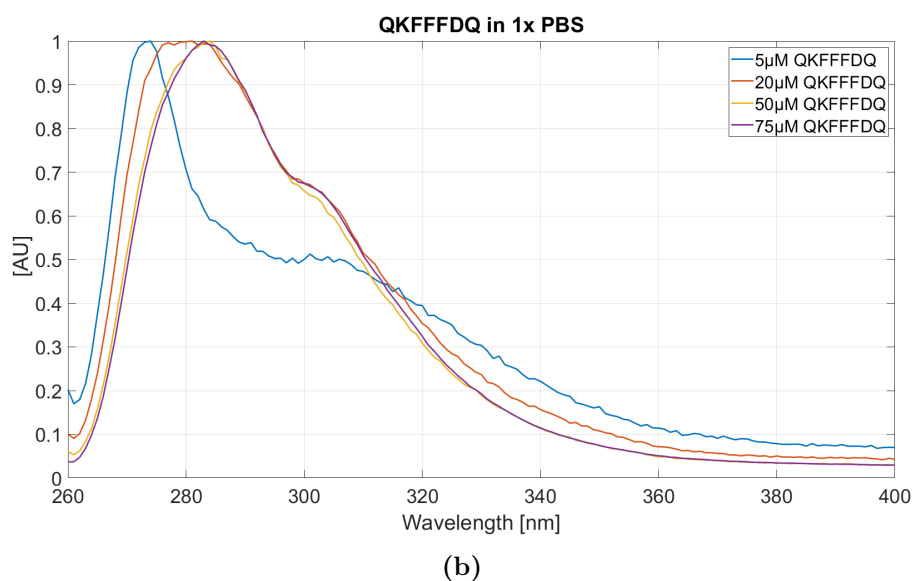


Figure 3.10: Emission spectra of (a) QDFFFKQ and (b) QKFFFDQ, in the range of 260-400nm. The excitation wavelength is 250nm. The spectra has been normalised. The solutions were prepared by dilution from a stock solution of $100\mu\text{M}$ with 1x PBS. A quartz cuvette with a path length of 1cm was used.

Fluorescence spectra of QDFFFKQ and QKFFFDQ (figure 3.10a and 3.10b shows a red-shift in fluorescence peak from 275nm to 285nm in correlation with increasing concentration. This can be attributed to an increasing number of Phe forming π -stacking, as π -stacking has been observed to cause shifts in the fluorescence spectrum, due to PET[47, 33]. No shift is observed between concentrations of $50\mu\text{M}$ and $75\mu\text{M}$, indicating that a final structure has been reached. These results also correspond to the CD spectra of the same peptides (figure 3.7a and 3.7b), where a major shift was observed between concentrations of $20\mu\text{M}$ and $50\mu\text{M}$. The peak around 303nm is likely the interaction of Phe with the solvent.[33]

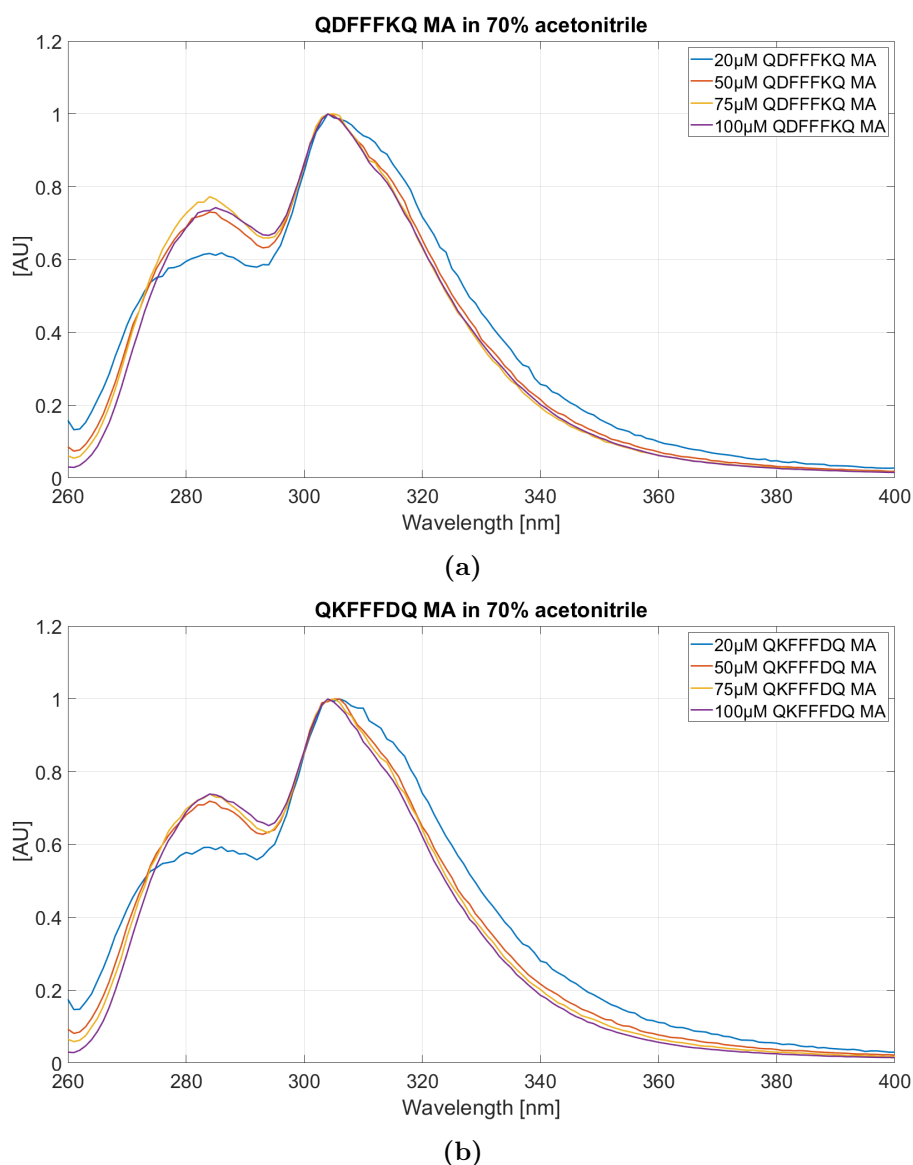


Figure 3.11: Emission spectra of QDFFFKQ MA (a) and QKFFFDQ MA (b), in the range of 260-400nm. The excitation wavelength is 250nm. The spectra has been normalised. The solutions were prepared by dilution from a stock solution of 100 μ M with 70% acetonitrile in water. A quartz cuvette with a path length of 1cm was used.

QDFFFKQ MA and QKFFFDQ MA (figure 3.11a and 3.11b) do not show a shift in fluorescent peak from 275nm to 285nm. Instead, it starts at 285nm, indicating that the peptides have already formed β -sheets, which corresponds to the CD spectra showing anti-parallel β -sheet structure at low concentrations (figure 3.8a and 3.8b). The relative fluorescent intensity of Phe also increases suddenly between 20 μ M and 50 μ M, which is likely due to the peptides forming larger supramolecular structures,

minimising contact with solvent, thus reducing interaction.

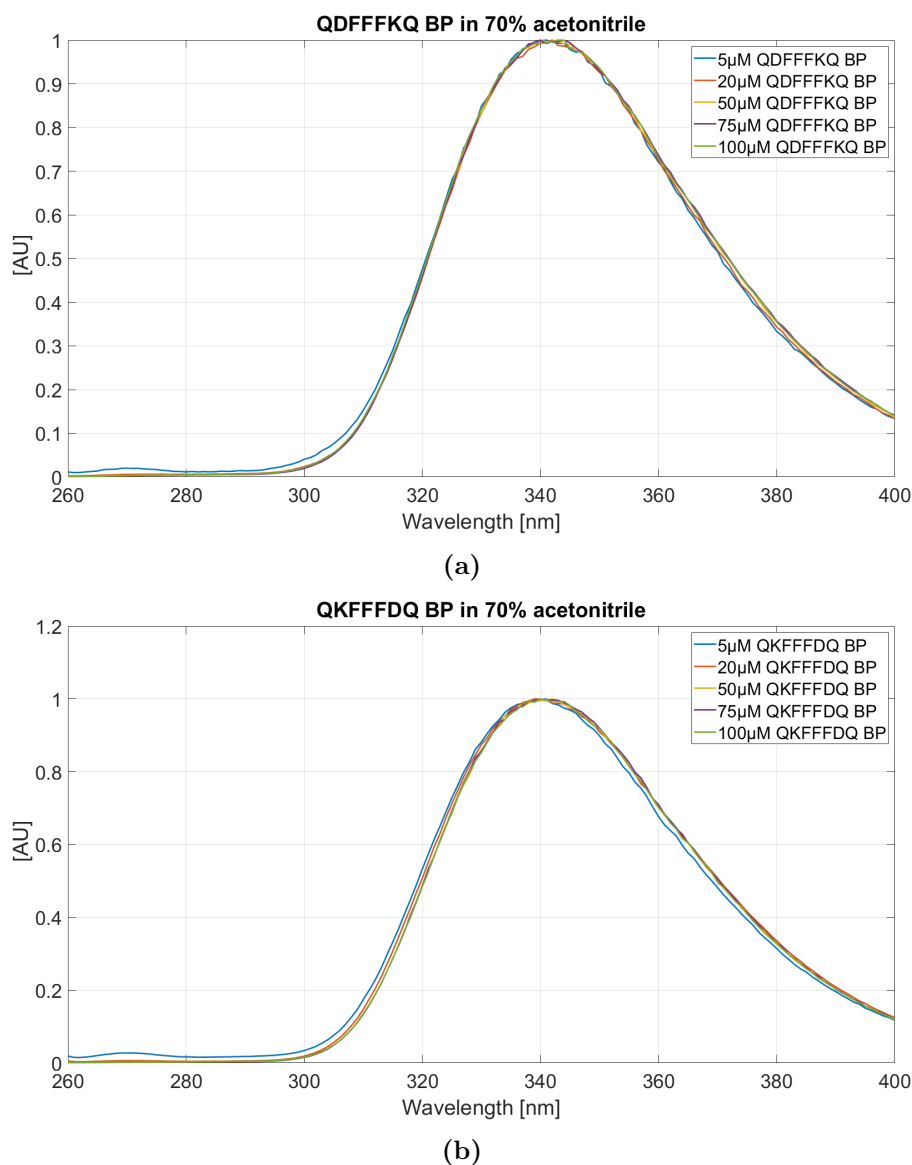


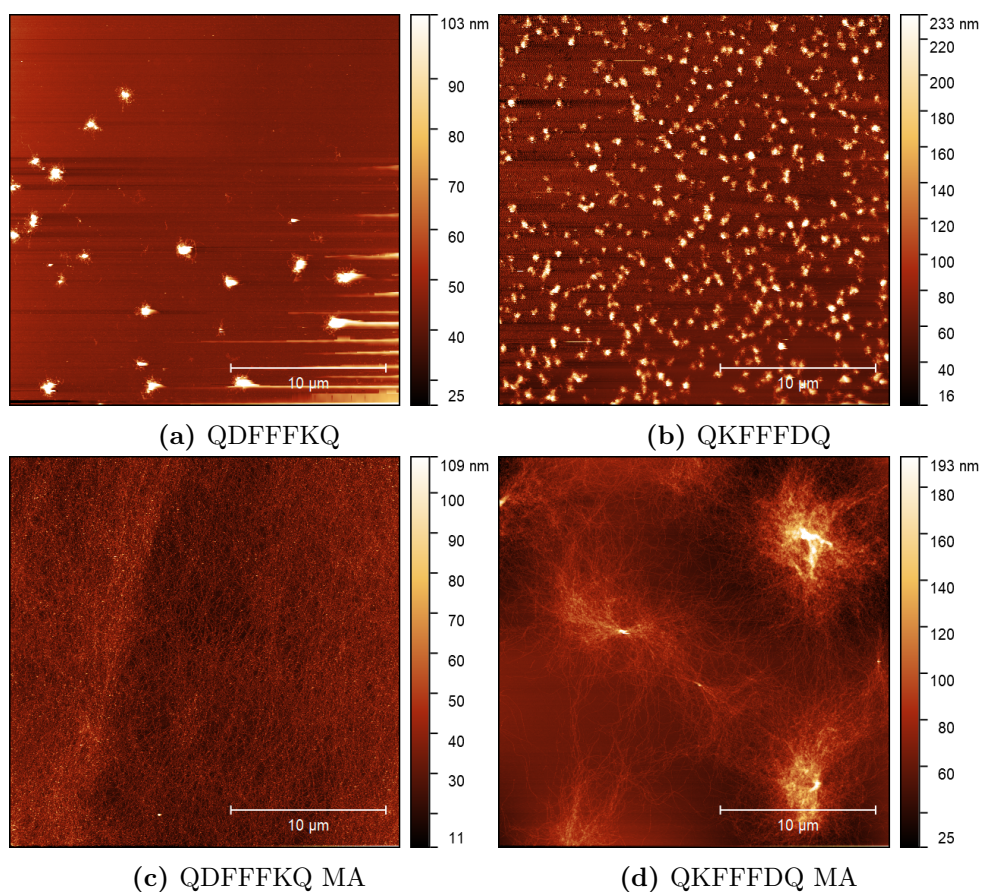
Figure 3.12: Emission spectra of QDFFFKQ BP (a) and QKFFFDQ BP (b), in the range of 260-400nm. The excitation wavelength is 250nm. The spectra has been normalised. The solutions were prepared by dilution from a stock solution of 100 μ M with 70% acetonitrile in water. A quartz cuvette with a path length of 1cm was used.

QDFFFKQ BP and QKFFFDQ BP (figure 3.12a and 3.12b) show no significant peak at the expected 285nm fluorescence of Phe, making it difficult to gain any insight into the self-assembly of the peptides. However, a massive peak is observed at 340nm, which correspond to the fluorescence observed for other biphenyl compounds[48].

This completely drowns the Phe peak, as the quantum yield of Phe is 0.022 compared to 0.18 of biphenyl[49].

The fluorescence data is in general agreement with CD data, as most samples show most conformational changes in the region 20-50 μ M. For further study, it would be of interest to analyse this region in detail, in order to determine if a critical fibre concentration exists. Another method, which could provide insight into the fibre formation is Thioflavin T fluorescence, as it has been suggested that the dye binds to an aromatic-hydrophobic groove of at least 4 β -strands[17, 43]. Furthermore, as the excitation and emission wavelengths are above 340nm emission peak of the biphenyl moiety, as observed by Slynborg et al.[17], it should be possible to also study QDFFFKQ BP and QKFFFDQ BP using this method.

3.7 AFM



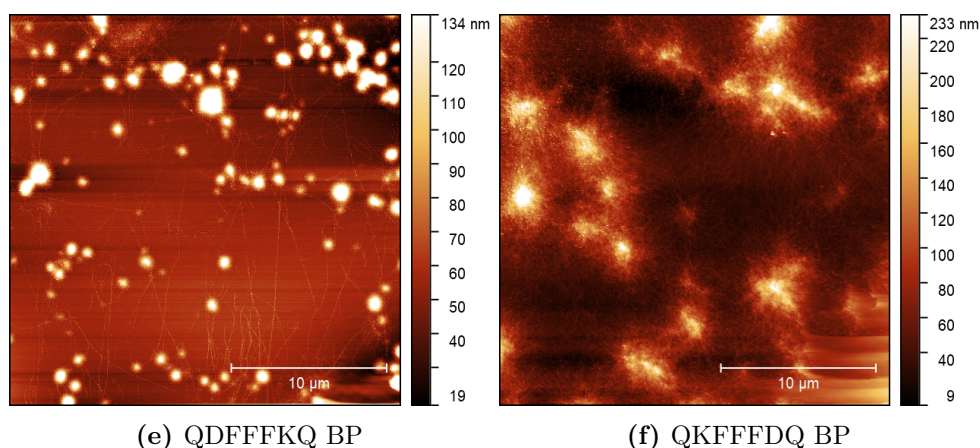


Figure 3.13: 25x25 μm AFM measurements of peptide deposited on silicon wafers (a) QDFFFKQ after 60 min (b) QKFFFDQ after 60 min (c) QDFFFKQ MA after 30 min (d) QKFFFDQ MA after 60 min (e) QDFFFKQ BP after 30 min (f) QKFFFDQ BP after 60 min

25x25 μm AFM measurements were made in order to compare structural differences between the different peptide samples (3.13). QDFFFKQ shows clusters of various sizes with small fibres extending out of the structures. The fibres are generally located in and around aggregates, however, a few single fibres can be observed away from the aggregates. QKFFFDQ have a high density of clusters of similar sizes. 5x5 μm images (Figure 3.15a) revealed small fibres extending out of the aggregates much like QDFFFKQ. QDFFFKQ MA shows a dense and evenly distributed network of fibres with no microscopic aggregates or clusters, whereas QKFFFDQ MA shows large clusters of fibres with a network of fibres connecting the clusters. As seen in the 5x5 μm image (figure 3.15d), QKFFFDQ MA forms aggregates after 30 min, which could explain the clusters observed after 60 min, as the aggregates serve as a medium for further fibrillation. Whether this effect is due to the structural differences between the two peptides or impurities in the sample can not be confirmed as the exact purity of the samples could not be determined by HPLC and TLC. QDFFFKQ BP shows clusters of various sizes, with long fibres going across the silicon wafer, connecting the clusters. QKFFFDQ BP shows a similar structure to QKFFFDQ MA, however, the clusters seem smaller with a higher density of fibres. As most of the surface was covered by structures like this, it was difficult to get images of single fibres.

In general, modifications of QDFFFKQ show distinct structural changes, whereas modifications of QKFFFDQ simply seem to increase the propensity of fibrillation. This could be explained by the MD simulations, as QKFFFDQ showed higher potential for fibrillation than QDFFFKQ. It is likely that QKFFFDQ MA and QKFFFDQ BP are still guided by the π -stacking of the backbone while the hydrophobic and aromatic moieties simply enforce fibrillation, whereas fibrillation of QDFFFKQ MA and QDFFFKQ BP are guided by the hydrophobic and aromatic moieties respectively. As a result, QDFFFKQ MA and QDFFFKQ BP show distinct differences in the

overall structure.

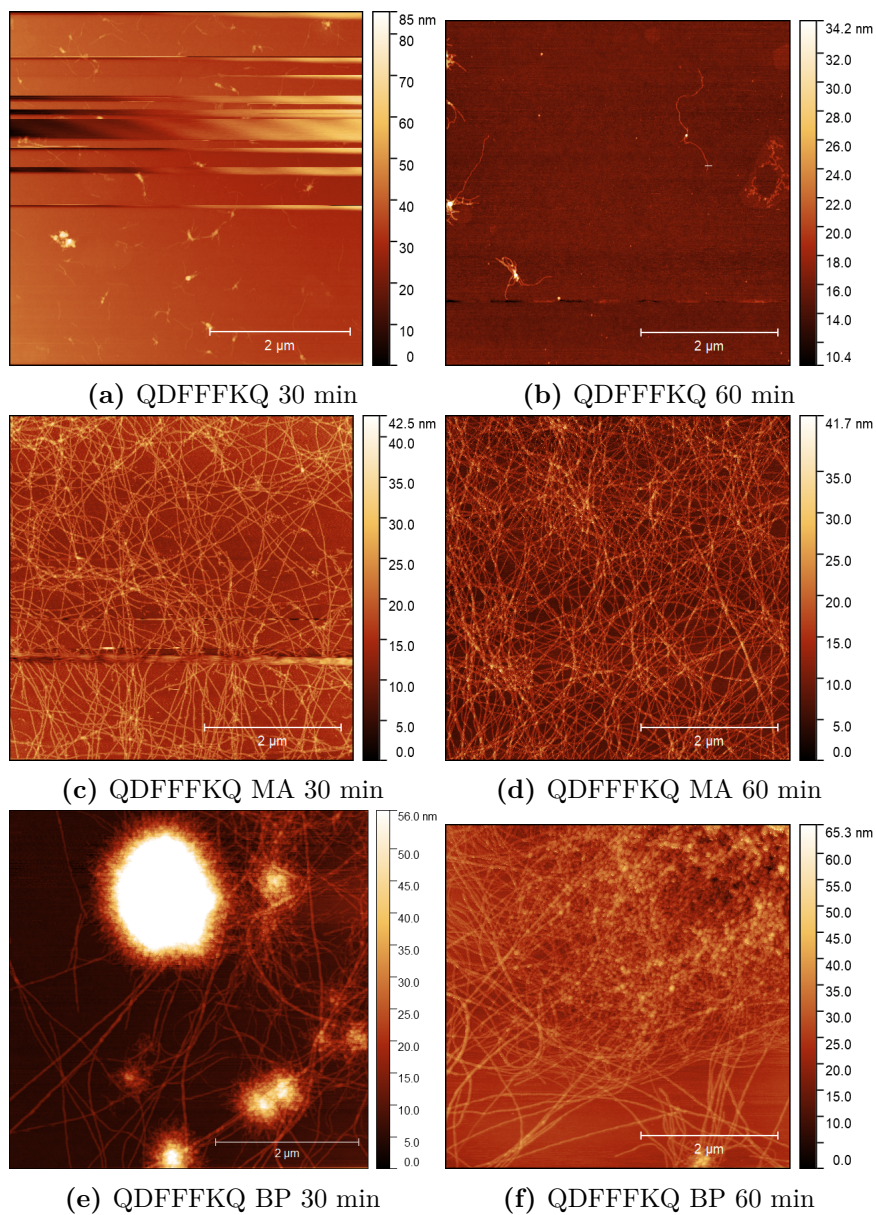


Figure 3.14: $5 \times 5 \mu\text{m}$ AFM measurements of peptide deposited on silicon wafers with different incubation times. QDFFFKQ incubated for (a) 30min and (b) 60min, QDFFFKQ MA incubated for (c) 30min and (d) 60min and QDFFFKQ BP incubated for (e) 30min and (f) 60min.

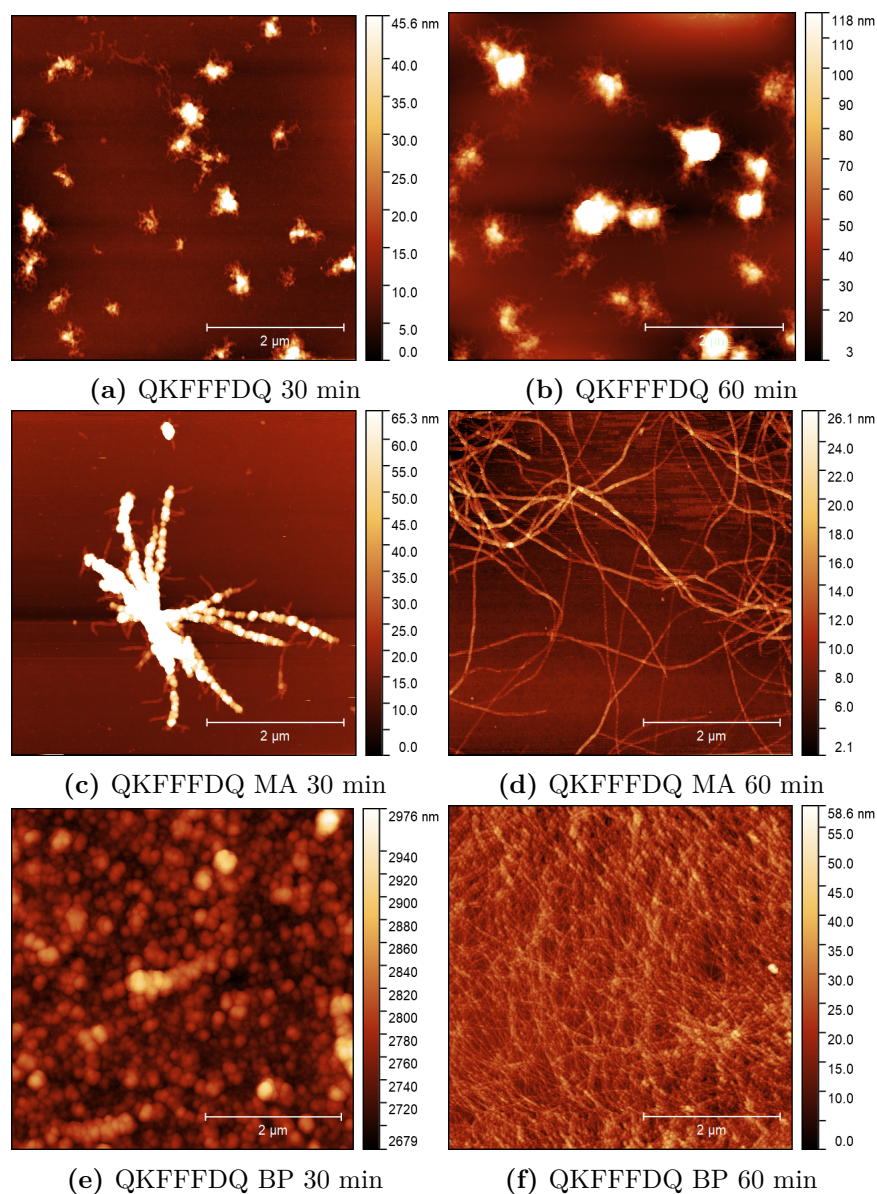


Figure 3.15: $5 \times 5 \mu\text{m}$ AFM measurements of peptide deposited on silicon wafers with different incubation times. QKFFFDQ incubated for (a) 30min and (b) 60min, QKFFFDQ MA incubated for (c) 30min and (d) 60min and QKFFFDQ BP incubated for (e) 30min and (f) 60min.

When looking at Figure 3.14 and 3.15 all peptides show a tendency to increase overall coverage, fibre length and cluster sizes. This is expected, as longer incubation time will increase the concentration of peptide on the wafer, as the solution slowly evaporates, due to the high concentration of acetonitrile. It is difficult to observe any structural changes in QKFFFDQ BP as the entire surface was covered by larger clusters and dense fibrillar networks. Additionally, the tip seems damaged, as some

of the fibres in figure 3.15f appear multiple times.

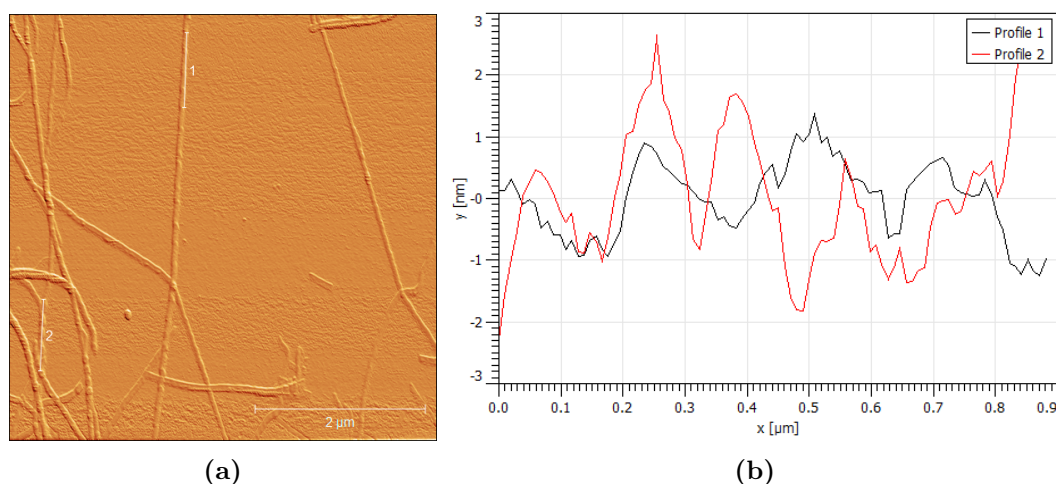


Figure 3.16: (a) Shaded 5x5µm AFM image of QDFFFKQ BP after 30min indicating helical structure in vertically aligned fibres. (b) Height profiles of the two marked lines from (a)

QDFFFKQ BP shows signs of helicity in fibres (figure 3.16), as bumps were observed along the fibre[43]. Profiles of fibres revealed periodic changes in height. Profile 1 shows a difference in height of 1.5-2nm over a period of 200nm. Profile 2 was taken of two fibres intertwining, showing roughly a doubling in height compared to profile 1. This phenomenon could not be observed in any of the other samples, as it was not possible to find any isolated, straight fibres. Assuming this helicity is present for all peptide samples, a variation of $\pm 1\text{nm}$ is expected for all fibres. Additionally, a statistical error of $\pm 0.2\text{nm}$ can be expected due to noise levels measured.

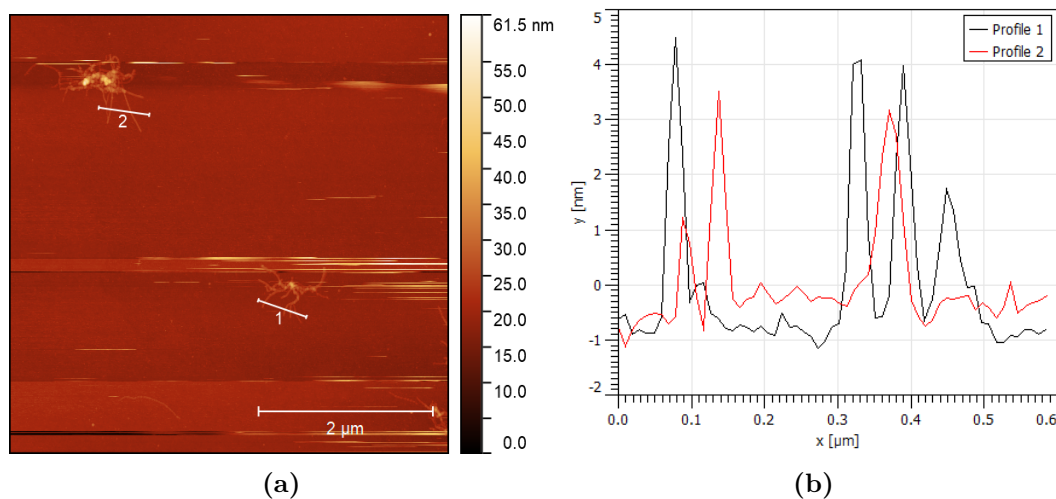


Figure 3.17: (a) 5x5µm AFM measurement of QDFFFKQ after 120min. (b) Height profile of the two marked lines from (a). The heights were determined using a bilateral minimum

Fibre sizes were measured by cross-section profiles of fibres found in $5 \times 5 \mu\text{m}$ AFM images (figure 3.17). The heights of the fibres were determined by utilising Gwyddions peak finder and bilateral minimum functions. The fibre heights of different peptide samples were measured and compiled into tables 3.2 and 3.3.

	QDFFFKQ	QDFFFKQ MA	QDFFFKQ BP
30 min	1.0, 1.0, 1.2, 3.2, 4.5 nm	3.0, 4.2, 5.6, 6.3, 6.4, 6.8, 7.5, 7.6 nm	3.3, 3.5, 6.9, 7.9, 9.8 nm
60 min	3.5, 3.7, 3.8, 4.3, 4.9, 5.2, 6.3, 7.6, 13.7 nm	3.5, 3.7, 3.8, 4.6, 5.6, 7.9, 6.6, 6.2 nm	8.7, 7.6, 6.1, 5.4, 5.6, 7.9, 6.6, 6.2 nm
120 min	5.0, 4.6, 5.1, 2.1, 3.7, 4.1, 2.0 nm	5.4, 5.9, 10, 8.9, 6.3, 6.2 nm	14.3, 4.9, 4.9, 6.3 nm

Table 3.2: Heights of fibres of QDFFFKQ, QDFFFKQ MA and QDFFFKQ BP after 30, 60 and 120min. Heights were determined by bilateral minimum. All AFM measurements and profiles used can be found in appendix A

	QKFFFDQ	QKFFFDQ MA	QKFFFDQ BP
30 min	3.3, 2.8, 2.3, 1.9, 6.7 nm	5.6, 15.5, 7.8 nm	No fibres
60 min	2.4, 2.3, 1.9, 3.4, 3.0 nm	1.9, 2.7, 2.1, 6.6, 2.0, 7.5, 3.5 nm	6.2, 3.3, 2.6, 2.9, 2.7 nm (double tip)
120 min	4.3, 3.1, 7.2 nm	2.2, 1.1, 1.2, 1.5, 6.6, 3.0, 2.6, 1.6, 1.3 nm	6.4, 4.7, 4.0, 3.8, 3.9, 3.7, 1.9, 12.9, 8.6, 8.5, 7.5, 6.0 nm

Table 3.3: Heights of fibres of QKFFFDQ, QKFFFDQ MA and QKFFFDQ BP after 30, 60 and 120min. Heights were determined by bilateral minimum. All AFM measurements and profiles used can be found in appendix A

All samples show a wide range of fibre sizes, however, due to the potential helicity of the fibres, it is difficult to determine how many single fibrils each fibre consists of. Additionally, as some of the samples showed a high density of fibres, it was difficult to isolate and measure single fibres. As such, some of the fibres are likely stacked on top of each other, artificially increasing the measured fibre size.

Incubation time does not appear to greatly affect overall fibre size, as small fibres are still observed after 60 and 120min. This indicates that new fibres are constantly formed as the concentration increase.

Extended strand structure of QDFFFKQ and QKFFFDQ were measured in YASARA and the backbone length was determined to be close to 2.3nm, while the peptide width was determined to be 1.2nm. Thus, any fibre sizes in this range can

likely be attributed to single tapes or fibrils. As most of the measured fibres were above this size, the fibres generally consist of multiple amyloid fibrils, indicating that fibrillation occurs in a similar way to the model for fibrillation proposed by Boden et al.[19], presented in section 1.1.

Chapter 4

Conclusion

N-terminal peptide modification was successfully carried out using an extension of SPSS with *in situ* carboxylic acid esterification of myristic acid and biphenyl-4-carboxylic acid. This shows potential as a simple method for synthetic modification of peptides. One important parameter is the solubility of the modification compound, as it was found that aggregation of activated esters inhibits coupling to the N-terminus of the peptide.

CD and fluorescence measurements indicate π -stacking in all peptides (with the exception of QDFFFKQ BP and QKFFFDQ BP fluorescence being dominated by biphenyl emission). characteristic CD spectra for beta-sheet secondary structure was also observed for QDFFFKQ MA and QKFFFDQ MA up to $20\mu\text{M}$, which disappears at $50\mu\text{M}$ as the peptides form larger supramolecular structures.

AFM measurements confirm that all peptides form fibres in polar solutions. Modifications were shown to significantly increase fibrillation of all peptides, while QDFFFKQ also showed major changes in overall fibrillation pattern depending on moiety.

One major problem with the modified peptides is the significant decrease in solubility in aqueous solutions, resulting in a need for high concentrations of acetonitrile. This makes them unfavourable for biomedical purposes. As such, modification with shorter hydrophobic tails should be explored.

Bibliography

- [1] P. Cudic. *Peptide Modifications to Increase Metabolic Stability and Activity*. Methods in Molecular Biology. Humana Press, 2013.
- [2] S. F. Hedegaard, M. Cárdenas, R. Barker, L. Jorgensen, and M. Van De Weert. Lipidation effect on surface adsorption and associated fibrillation of the model protein insulin. *Langmuir*, 32(28):7241–9, jul 2016.
- [3] L. B. Knudsen, P. F. Nielsen, P. O. Huusfeldt, N. L. Johansen, K. Madsen, F. Z. Pedersen, H. Thøgersen, M. Wilken, and H. Agersø. Potent derivatives of glucagon-like peptide-1 with pharmacokinetic properties suitable for once daily administration. *Journal of medicinal chemistry*, 43(9):1664–1669, may 2000.
- [4] S. Havelund, A. Plum, U. Ribel, I. Jonassen, A. Vølund, J. Markussen, and P. Kurtzhals. The mechanism of protraction of insulin detemir, a long-acting, acylated analog of human insulin. *Pharmaceutical Research*, 21(8):1498–1504, 2004.
- [5] C. M. A. Martin, N. Irwin, P. R. Flatt, and V. A. Gault. A novel acylated form of (d-ala²)gip with improved antidiabetic potential, lacking effect on body fat stores. *BBA - General Subjects*, 1830(6):3407–3413, jun 21013.
- [6] E. Longo, E. Santis, R. Hussain, C. F. van der Walle, J. Casas-Finet, S. Uddin, A. Santos, and G. Siligardi. The effect of palmitoylation on the conformation and physical stability of a model peptide hormone. *International Journal of Pharmaceutics*, 472(1-2):156–164, sep 2014.
- [7] B. P. Ward, N. L. Ottaway, D. Perez-Tilve, D. Ma, V. M. Gelfanov, M. H. Tschöp, and R. D. Dimarchi. Peptide lipidation stabilizes structure to enhance biological function. *Molecular Metabolism*, 2(4):468–479, 2013.
- [8] P. Roach, D. Farrar, and C. C. Roach. Interpretation of protein adsorption: surface-induced conformational changes. *Journal of the American Chemical Society*, 127(22):8168–8173, jun 2005.
- [9] T. Zoungrana, G. H. Findenegg, and W. Norde. Structure, stability, and activity of adsorbed enzymes. *Journal of Colloid And Interface Science*, 190(2):437–448, jun 1997.

- [10] G. Fichman and E. Cazit. Self-assembly of short peptides to form hydrogels: Design of building blocks, physical properties and technological applications. *Acta Biomaterialia*, 10(4):1671–1682, apr 2014.
- [11] C. J. Bowerman and B. L. Nilsson. Self-assembly of amphipathic β -sheet peptides: insights and applications. *Biopolymers*, 98(3):169–84, 2012.
- [12] S. Van Vlierberghe, P. Dubruel, and E. Schacht. Biopolymer-based hydrogels as scaffolds for tissue engineering applications: a review. *Biomacromolecules*, 12(5):1387–1408, may 2011.
- [13] J. L. Drury and D. J. Mooney. Hydrogels for tissue engineering: scaffold design variables and applications. *Biomaterials*, 24(24):4337–4351, 2003.
- [14] Y. Qiu and K. Park. Environment-sensitive hydrogels for drug delivery. *Advanced Drug Delivery*, 64:49–60, dec 2012.
- [15] M. W. Tibbitt and K. S. Anseth. Hydrogels as extracellular matrix mimics for 3d cell culture. *Biotechnology and Bioengineering*, 103(4):655–663, jul 2009.
- [16] N. A. Peppas, J. Z. Hilt, A. Khademhosseini, and R. Langer. Hydrogels in biology and medicine: From molecular principles to bionanotechnology. *Advanced Materials*, 18(11):1345–1360, jun 2006.
- [17] M. Slynngborg, D. A. Nielsen, and P. Fojan. The physical properties and self-assembly potential of the rfffr peptide. *ChemBioChem*, 17(21):2083–2092, nov 2016.
- [18] A. Aggeli, M. Bell, N. Boden, J. N. Keen, T. C. B. McLeish, I. E. Nyrkova, S. E. Radford, and A. N. Semenov. Engineering of peptide β -sheet nanotapes. *Journal of Materials Chemistry*, 7(7):1135–1145, 1997.
- [19] A. Aggeli, I. A. Nyrkova, M. Bell, R. Harding, L. Carrick, T. C. B. McLeish, A. N. Semenov, and N. Boden. Hierarchical self-assembly of chiral rod-like molecules as a model for peptide β -sheet tapes, ribbons, fibrils, and fibers. *Proceedings of the National Academy of Sciences of the United States of America*, 98(21):11857–11862, oct 2001.
- [20] M. Slynngborg and P. Fojan. A computational study of the self-assembly of the rfffr peptide. *Physical Chemistry Chemical Physics*, 17(44):30023–30036, 2015.
- [21] D. C. Rapaport and D. Rapaport. *The Art of Molecular Dynamics Simulation*. Cambridge University Press, second edition, jan 2004.
- [22] D. Frenkel and B. Smit. *Understanding Molecular Simulation : From Algorithms to Applications*, volume v. 1 of *Computational science series*. Elsevier Science & Technology, second edition, oct 2001.

- [23] S. J. Marrink and D. P. Tieleman. Perspective on the martini model. *Chemical Society Reviews*, 42(16):6801–6822, 2013.
- [24] S. L. Pedersen K. J. Jensen, P. Tofteng Shelton. *Peptide Synthesis and Applications*. Humana Press Inc., second edition, 2013.
- [25] H. Jiang, X. Zhang, X. Chen, P. Aramsangtienchai, Z. Tong, and H. Lin. Protein lipidation: Occurrence, mechanisms, biological functions, and enabling technologies. *Chemical reviews*, 118(3):919–988, feb 2018.
- [26] P. Berndt, G. B. Fields, and M. Tirrell. Synthetic lipidation of peptides and amino acids monolayer structure and properties. *Journal of the American Chemical Society*, 117(37):9515–9522, sep 1995.
- [27] J. Lorsch. *Facet navigation Title Laboratory methods in enzymology: cell, lipid and carbohydrate*, volume 533 of *Methods in enzymology*. Academic Press, first edition, dec 2013.
- [28] B. Fried and J. Sherma. *Thin-Layer Chromatography*, volume 81 of *Chromatographic Science*. CRC Press LLC, fourth edition, mar 1999.
- [29] J. H Gross. *Mass Spectrometry*. Springer International Publishing, third edition, 2017.
- [30] D. S. Rodgers and S. C. Wilhite. *Circular Dichroism: Theory and Spectroscopy*. Biochemistry Research Trends. Nova Science Publishers, Incorporated, first edition, jan 2011.
- [31] S. M. Kelly, T. J. Jess, and N. S. C. Price. How to study proteins by circular dichroism. *Biochimica et biophysica acta*, 1751 2:119–39, 2005.
- [32] J. R. Lakowicz. *Principles of Fluorescence Spectroscopy*. Springer US, third edition, 2006.
- [33] S. Doose, H. Neuweiler, and M. Sauer. Fluorescence quenching by photoinduced electron transfer: A reporter for conformational dynamics of macromolecules. *ChemPhysChem*, 10(9-10):1389–1398, jul 2009.
- [34] P. Eaton and P. West. *Atomic Force Microscopy*. Oxford University Press, 2010.
- [35] P. C. Braga and D. Ricci. *Atomic Force Microscopy: Biomedical Methods and Applications*, volume 242. Humana Press, 2003.
- [36] S. Pronk, S. Páll, R. Schulz, P. Larsson, P. Bjelkmar, R. Apostolov, M.R. Shirts, J.C. Smith, P.M. Kasson, D. Van Der Spoel, B. Hess, and E. Lindahl. Gromacs 4.5: a high-throughput and highly parallel open source molecular simulation toolkit. *Bioinformatics*, 29(7):845–854, 2013.

- [37] D. H. de Jong, G. Singh, W. F. D. Bennet, C. Arnarez, T. A. Wassenaar, L. V. Schafer, X. Periole, D.P. Tieleman, and S.J. Marrink. Improved parameters for the martini coarse-grained protein force field. *Journal of Chemical Theory and Computation*, 9(1):687–697, 2013.
- [38] S. O. Yesylevskyy, L. V. Schafer, D. Sengupta, and S. J. Marrink. Polarizable water model for the coarse-grained martini force field (polarizable coarse-grained water). *PLoS Computational Biology*, 6(6):e10008210, 2010.
- [39] W. Humphrey, A. Dalke, and K. Schulten. Vmd: Visual molecular dynamics. *Journal of Molecular Graphics*, 14(1):33–38, 1996.
- [40] A. C. E. Dahl, M. Chavent, and M. S. P. Sansom. Bendix: intuitive helix geometry analysis and abstraction. *Bioinformatics*, 28(16):2193–2194, 2012.
- [41] D. Nečas and P. Klapetek. Gwyddion: an open-source software for SPM data analysis. *Central European Journal of Physics*, 10:181–188, 2012.
- [42] A. M. Smith, R. J. William, C. Tang, P. Coppo, R. F. Collins, M. L. Turner, A. Saiani, and R. V. Ulijn. Fmoc-diphenylalanine self assembles to a hydrogel via a novel architecture based on π - π interlocked β -sheets. *Advanced Materials*, 20(1):37–41, jan 2008.
- [43] S. Marchesan, C. D. Easton, F. Kushkaki, L. Waddington, and P. G. Hartley. Tripeptide self-assembled hydrogels: unexpected twists of chirality. *Chemical Communications*, 48(16):2195–2197, 2012.
- [44] S. Marchesan, Y. Qu, L. J. Waddington, C. D. Easton, V. Glattauer, T. J. Lithgow, K. M. Mclean, J. S. Forsythe, and P. G. Hartley. Self-assembly of ciprofloxacin and a tripeptide into an antimicrobial nanostructured hydrogel. *Biomaterials*, 34(14):3678–3687, may 2013.
- [45] S. Marchesan, K. E. Styan, C. D. Easton, L. Waddington, and A. V. Vargiu. Higher and lower supramolecular orders for the design of self-assembled heterochiral tripeptide hydrogel biomaterials. *Journal of Materials Chemistry B*, 3(41):8123–9132, 2015.
- [46] N. J. Greenfield. Using circular dichroism spectra to estimate protein secondary structure. *Nature protocols*, 1(6):2876–2890, 2006.
- [47] S. Doose, H. Neuweiler, and M. Sauer. A close look at fluorescence quenching of organic dyes by tryptophan. *ChemPhysChem*, 6(11):2277–2285, nov 2005.
- [48] J. W. Bridges, P. J. Creaven, and R. T. Williams. The fluorescence of some biphenyl derivatives. *The Biochemical journal*, 96(3):872–878, sep 1965.
- [49] M. Taniguchi and J. S. Lindsey. Database of absorption and fluorescence spectra of >300 common compounds for use in photochemcad. *Photochemistry and Photobiology*, 94(2):290–327, mar 2018.

Appendix A

A.1 AFM

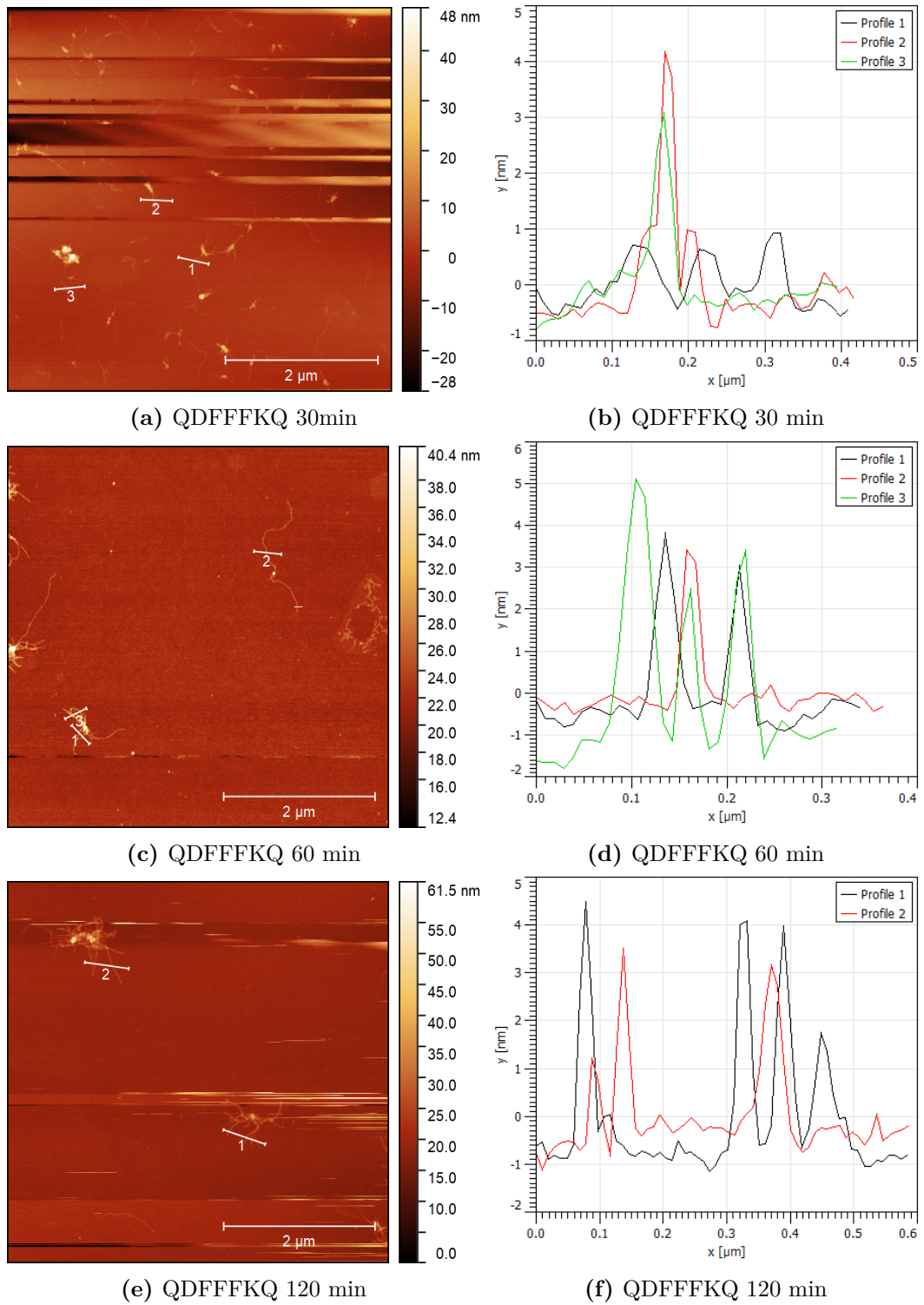
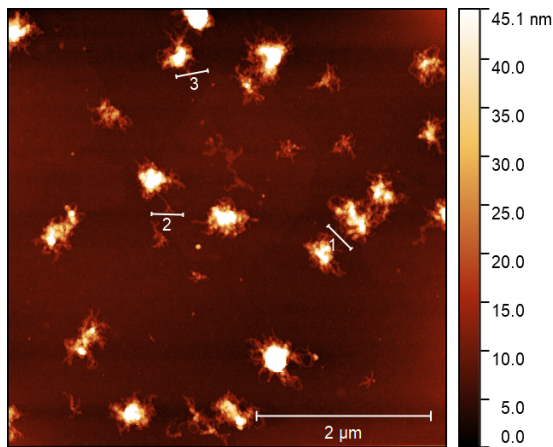
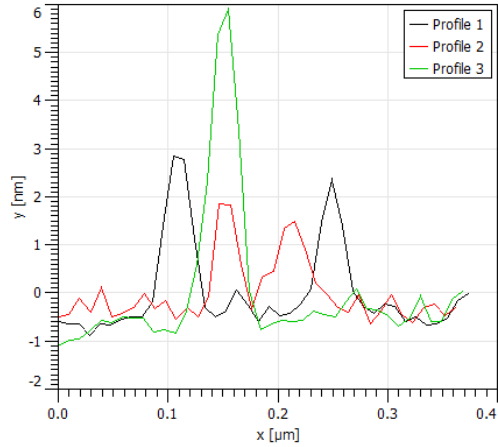


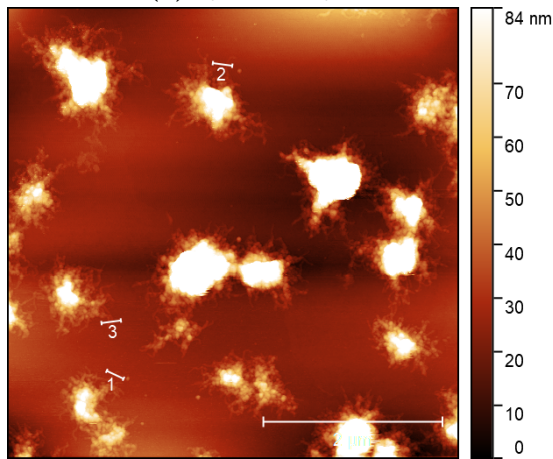
Figure A.1: $5 \times 5 \mu\text{m}$ AFM measurement of QDFFFKQ with height profiles.



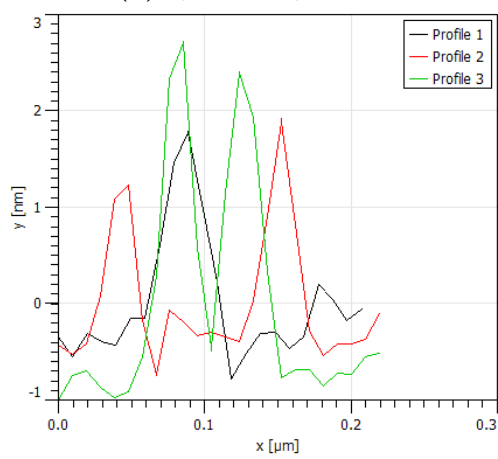
(a) QKFFFDQ 30min



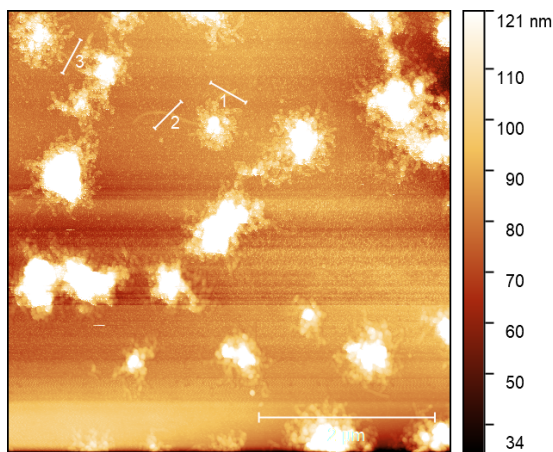
(b) QKFFFDQ 30 min



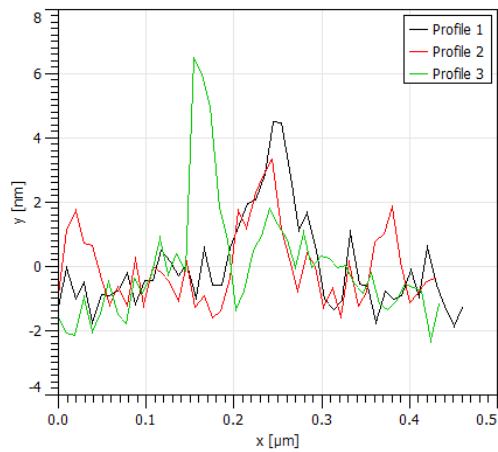
(c) QKFFFDQ 60 min



(d) QKFFFDQ 60 min



(e) QKFFFDQ 120 min



(f) QKFFFDQ 120 min

Figure A.2: 5x5 μ m AFM measurement of QKFFFDQ with height profiles.

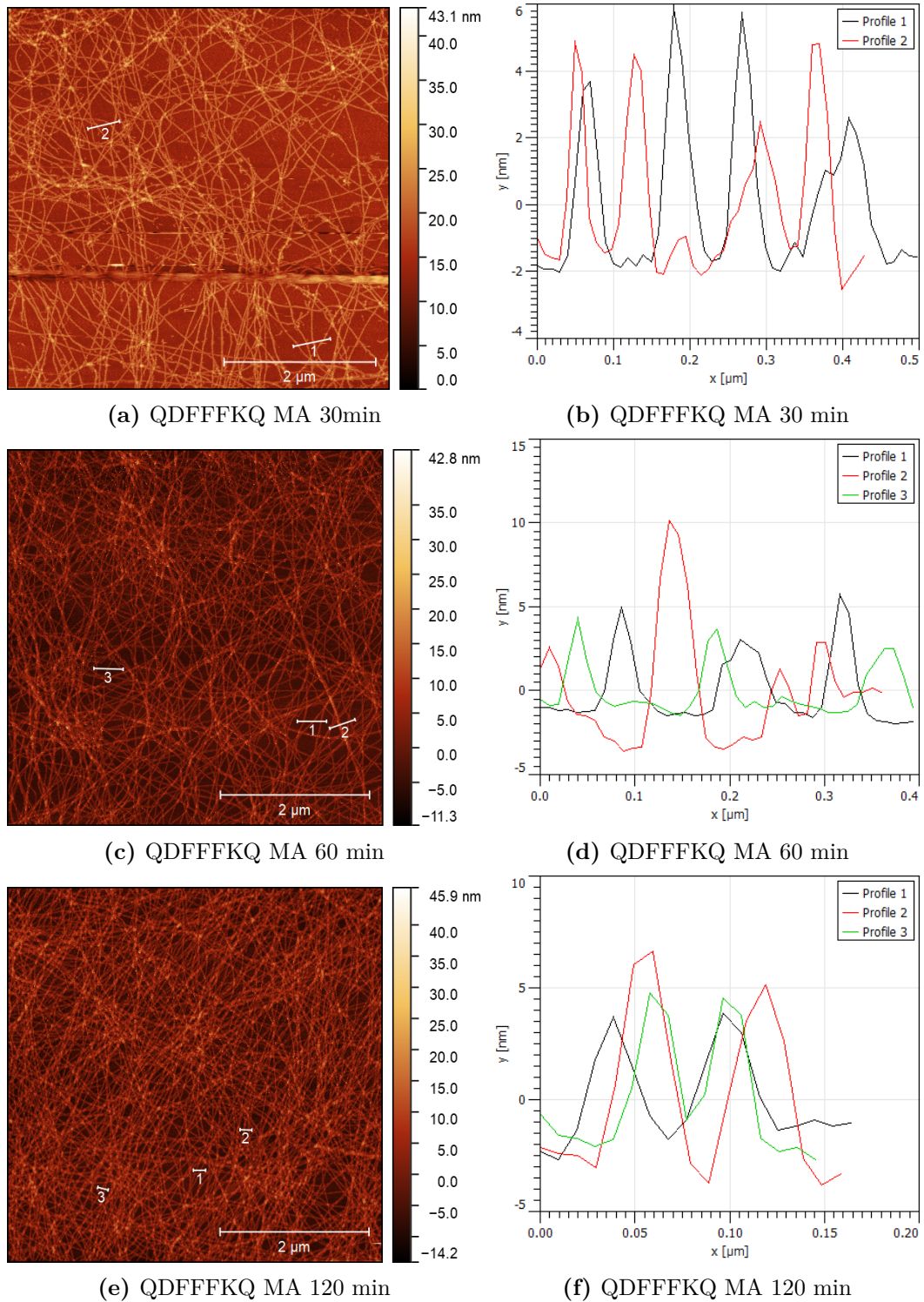
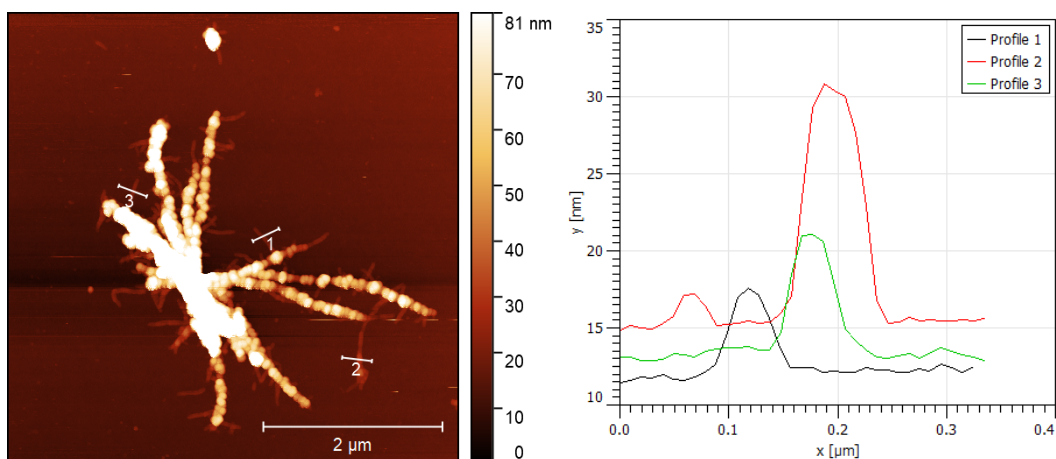
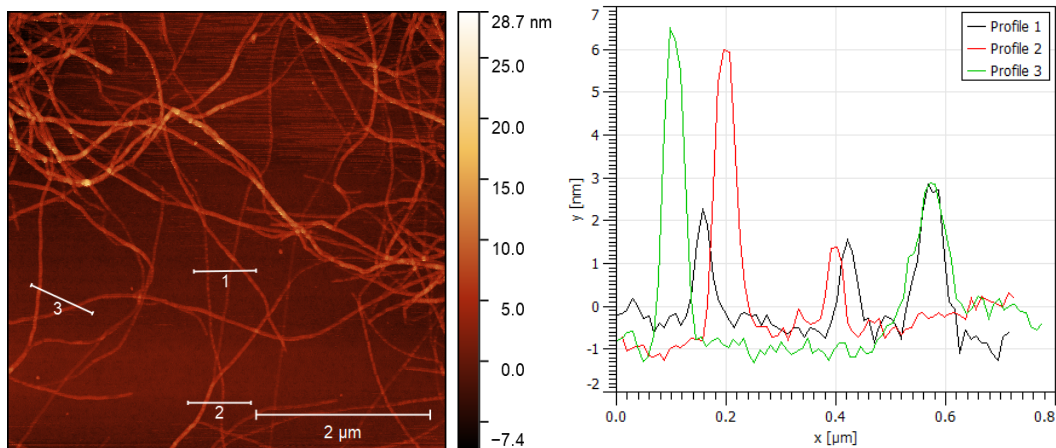


Figure A.3: $5 \times 5 \mu\text{m}$ AFM measurement of QDFFFKQ MA with height profiles.



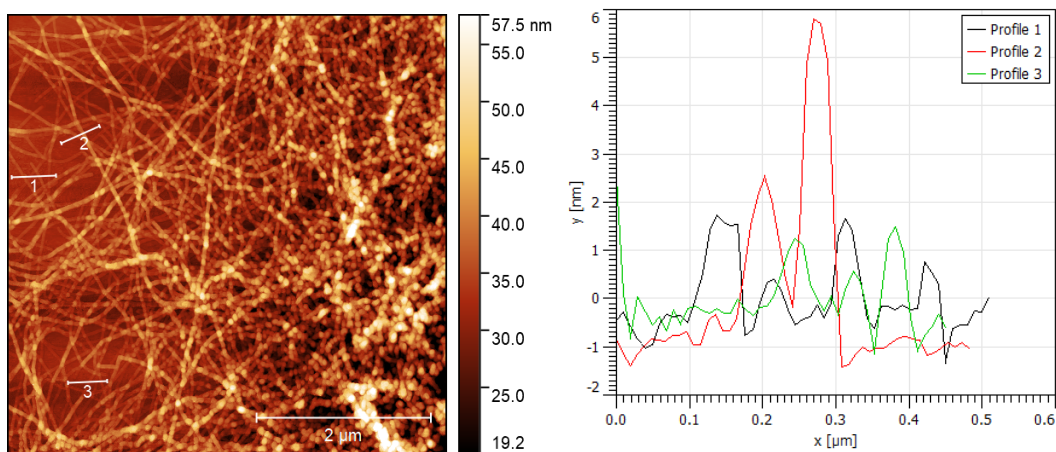
(a) QKFFFDQ MA 30min

(b) QKFFFDQ MA 30 min



(c) QKFFFDQ MA 60 min

(d) QKFFFDQ MA 60 min



(e) QKFFFDQ MA 120 min

(f) QKFFFDQ MA 120 min

Figure A.4: 5x5 μm AFM measurement of QKFFFDQ MA with height profiles.

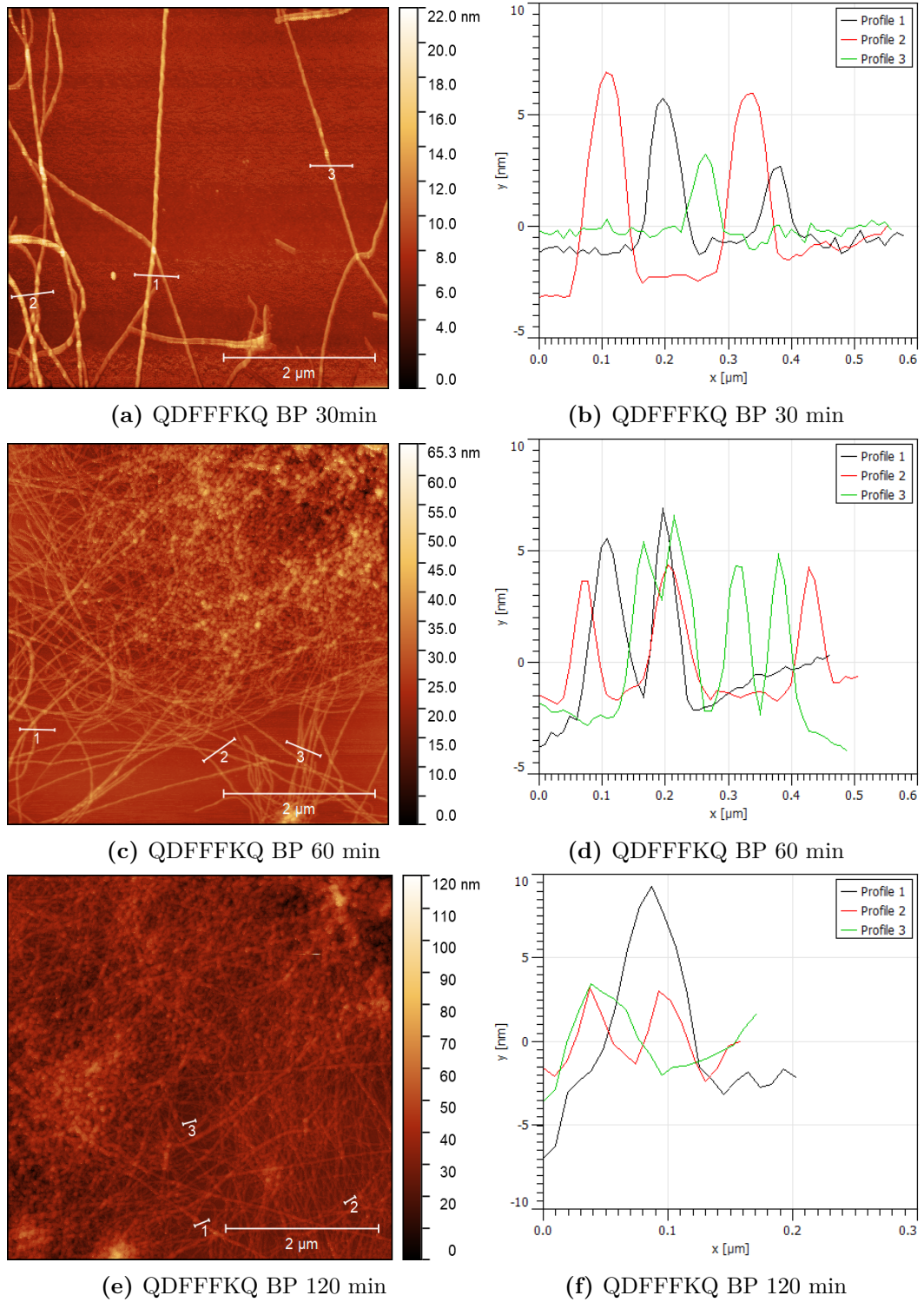
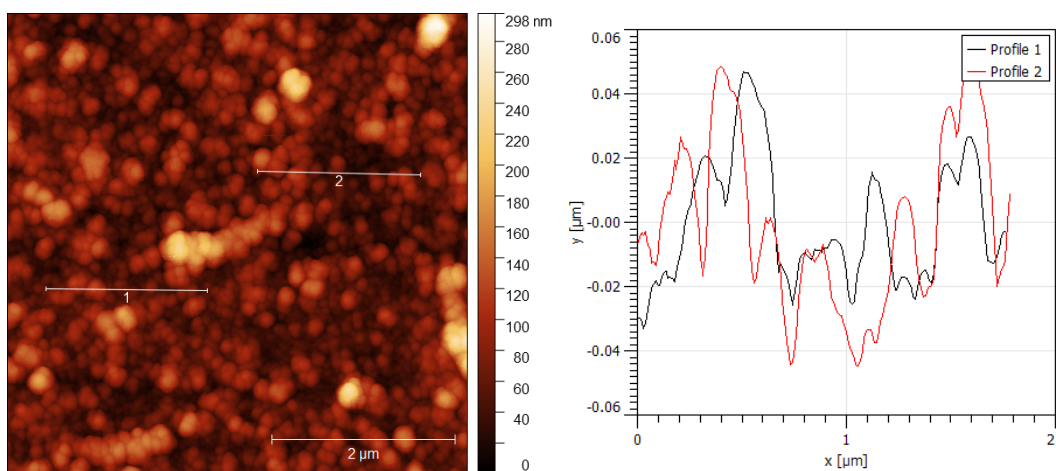
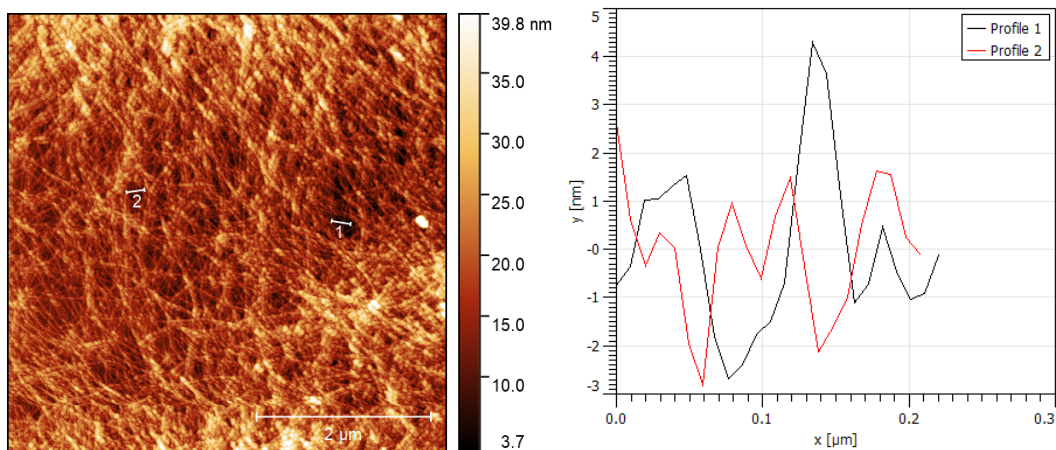


Figure A.5: $5 \times 5 \mu\text{m}$ AFM measurement of QDFFFKQ BP with height profiles.



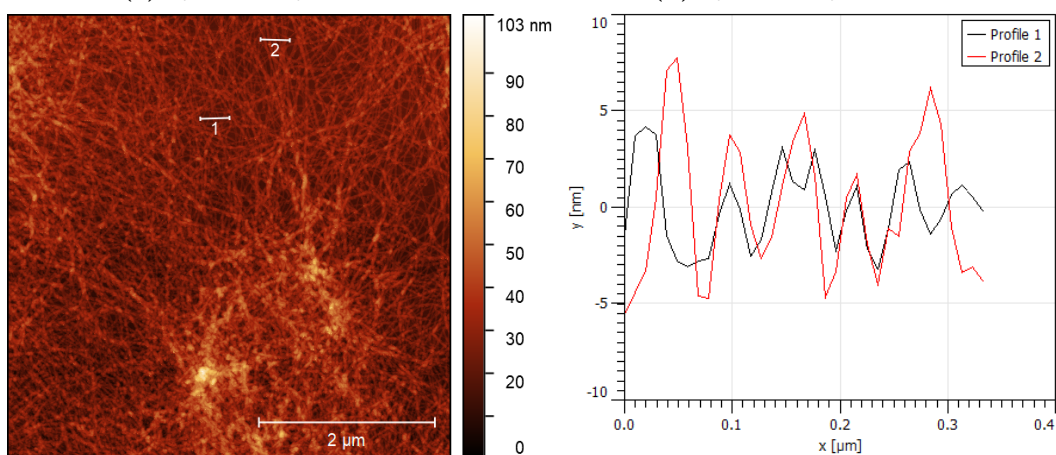
(a) QKFFFDQ BP 30min

(b) QKFFFDQ BP 30 min



(c) QKFFFDQ BP 60 min

(d) QKFFFDQ BP 60 min



(e) QKFFFDQ BP 120 min

(f) QKFFFDQ BP 120 min

Figure A.6: 5x5 μm AFM measurement of QKFFFDQ BP with height profiles.